PHYSICAL REVIEW D **87,** 094022 (2013)

Open charm production at the LHC: k_t-factorization approach

Rafał Maciuła*
Institute of Nuclear Physics PAN, PL-31-342 Cracow, Poland

Antoni Szczurek†
Institute of Nuclear Physics PAN, PL-31-342 Cracow, Poland and University of Rzeszów, PL-35-959 Rzeszów, Poland
(Received 22 January 2013; published 21 May 2013)

We discuss inclusive production of open charm in proton-proton scattering at LHC. The calculation is performed within the k_t-factorization approach. Different models of unintegrated gluon distributions (UGDFs) from the literature are used. The theoretical transverse momentum as well as (pseudo)rapidity distributions of charmed mesons are compared with recent experimental data of the ATLAS, ALICE, and LHCb Collaborations. Only the calculation with Kimber-Martin-Ryskin UGDF gives results comparable to experimental ones. All other popular models of UGDF significantly underpredict experimental data. Several sources of uncertainties of the theoretical predictions are also studied in detail. In addition, we discuss correlations between D and $\bar{D}$ mesons. Good description of experimental distribution in invariant mass and in relative azimuthal angle between D and $\bar{D}$ mesons is achieved for the Kimber-Martin-Ryskin UGDF. The considered correlation observables measured by the LHCb experiment were not discussed in other approaches in the literature

DOI: 10.1103/PhysRevD.87.094022 PACS numbers: 13.87.Ce, 14.65.Dw

I. INTRODUCTION

At high-energy hadronic scattering, gluon-gluon fusion is known to be the dominant mechanism of open charm production. Even at RHIC the contribution from quark-antiquark annihilation constitutes only a small fraction of the cross section. Usually in the studies of heavy quark production, the main efforts concentrate on inclusive distributions. The transverse momentum distribution of charmed mesons is the best example. The standard collinear next-to-leading-order (NLO) approach [1] as well as its improved schemes, e.g., fixed-order plus next-to-leading logarithms (FONLL) [2] or general-mass variable-flavour-number scheme [3], are state of the art in this respect. These approaches cannot be, however, used when transverse momenta of the charm quark and antiquark are not equal. This means in practice that it cannot be used for studies of correlation observables for charmed meson pairs or for meson-nonphotonic electron modes.

The k_t-factorization approach seems a much more efficient tool in this respect [4–11]. Different unintegrated gluon distributions (UGDFs) in the proton have been used in the literature in this context [12–16]. Recently, we have applied this formalism to the description of inclusive distributions of so-called nonphotonic electrons [17] and electron-positron correlations [18] at RHIC. A rather good description of correlation observables has been achieved there.

The quark mass is sufficiently large to apply perturbative calculation but still small enough that interesting low-x effects may appear, too. In the k_t-factorization approach, the latter effects are contained in the unintegrated gluon distributions—the building blocks of the formalism. In principle, a comparison of experimental data and predictions with the UGDFs which include such effects may tell us more about footprints of the saturation effects—a topic extensively discussed in recent years.

Recently, the ATLAS [19], ALICE [20,21], and LHCb [22] Collaborations have measured inclusive distributions (mainly transverse momentum distributions) of different charmed mesons. The LHCb Collaboration has measured in addition a few correlation observables for charmed mesons for the first time in history in the forward rapidity region [23]. The STAR Collaboration at RHIC has measured correlation of charmed mesons and nonphotonic electrons [24]. At RHIC a study of meson-meson correlations was not possible due to limited statistics caused by relatively small cross sections. It was accessible only at the Tevatron, where the first midrapidity measurements of azimuthal angle correlations between charmed mesons have been performed by the CDF experiment [25].

In the present paper, we concentrate first on inclusive distributions of charmed mesons in order to test different models of unintegrated gluon distributions from the literature. Next we focus on $D\bar{D}$ meson correlations. Conclusions will close our paper.

II. SKETCH OF THE FORMALISM

The cross section for the production of a pair of charm quark—charm antiquark can be written as

*rafal.maciula@ifj.edu.pl
†antoni.szczurek@ifj.edu.pl

 © 2013 American Physical Society

$$\frac{d\sigma(pp\to c\bar{c}X)}{dy_1 dy_2 d^2p_{1t} d^2p_{2t}} = \frac{1}{16\pi^2\hat{s}^2}\int \frac{d^2k_{1t}}{\pi}\frac{d^2k_{2t}}{\pi}\overline{|\mathcal{M}^{\rm off}_{g^*g^*\to c\bar{c}}|^2} \times \delta^2(\vec{k}_{1t}+\vec{k}_{2t}-\vec{p}_{1t}-\vec{p}_{2t}) \times \mathcal{F}_g(x_1,k_{1t}^2,\mu^2)\mathcal{F}_g(x_2,k_{2t}^2,\mu^2). \tag{2.1}$$

The main ingredients in the formula are off-shell matrix elements for the $g^*g^* \to c\bar{c}$ subprocess and UGDFs. The relevant matrix elements are known and can be found in Refs. [26–28]. The unintegrated gluon distributions are functions of longitudinal momentum fraction x_1 or x_2 of the gluon with respect to its parent nucleon and of gluon transverse momenta k_t. Some of them depend in addition on the factorization scale μ. The longitudinal momentum fractions can be calculated as

$$x_1 = \frac{m_{1t}}{\sqrt{s}}\exp(y_1) + \frac{m_{2t}}{\sqrt{s}}\exp(y_2), \qquad x_2 = \frac{m_{1t}}{\sqrt{s}}\exp(-y_1) + \frac{m_{2t}}{\sqrt{s}}\exp(-y_2), \tag{2.2}$$

where $m_{it} = \sqrt{p_{it}^2 + m_Q^2}$ is the transverse mass of the produced quark or antiquark.

Various unintegrated gluon distributions have been discussed in the literature [12–16]. In contrast to the collinear gluon distributions (PDFs), they differ considerably among themselves. One may expect that they will lead to different production rates of $c\bar{c}$ pairs at the LHC. Since the production of charm quarks is known to be dominated by gluon-gluon fusion, charm production at the LHC can be used to verify the quite different models of UGDFs.

Below, we concentrate for a while on the Kimber-Martin-Ryskin (KMR) unintegrated gluon distribution, which, as will be discussed in this paper, gives the best description of the LHC experimental data, taking into account also correlation observables.

According to the KMR approach, the unintegrated gluon distribution is given by the following formula:

$$f_g(x,k_t^2,\mu^2) \equiv \frac{\partial}{\partial \log k_t^2}[g(x,k_t^2)T_g(k_t^2,\mu^2)] = T_g(k_t^2,\mu^2)\frac{\alpha_S(k_t^2)}{2\pi}\sum_b \int_x^1 dz P_{gb}(z) b\left(\frac{x}{z},k_t^2\right). \tag{2.3}$$

This definition is fully satisfied for $k_t > \mu_0$, where $\mu_0 \sim 1$ GeV is the minimum scale for which Dokshitzer-Gribov-Lipatov-Altarelli-Parisi (DGLAP) evolution of the conventional collinear gluon distributions, $g(x,\mu^2)$, is valid.

The virtual (loop) contributions may be resummed to all orders by the Sudakov form factor

$$T_g(k_t^2,\mu^2) \equiv \exp\left(-\int_{k_t^2}^{\mu^2}\frac{d\kappa_t^2}{\kappa_t^2}\frac{\alpha_S(\kappa_t^2)}{2\pi}\sum_b\int_0^1 dz z P_{bg}(z)\right), \tag{2.4}$$

which gives the probability of evolving from a scale k_t to a scale μ without parton emission.

The exponent of the gluon Sudakov form factor can be simplified by using the following identity: $P_{qg}(1-z) = P_{qg}(z)$. Then the gluon Sudakov form factor is

$$T_g(k_t^2,\mu^2) = \exp\left(-\int_{k_t^2}^{\mu^2}\frac{d\kappa_t^2}{\kappa_t^2}\frac{\alpha_S(\kappa_t^2)}{2\pi} \times \left(\int_0^{1-\Delta} dz z P_{gg}(z) + n_F\int_0^1 dz P_{qg}(z)\right)\right), \tag{2.5}$$

where n_F is the quark-antiquark active number of flavors into which the gluon may split and $\Delta = k_t/(k_t+\mu)$, which introduces a restriction of the phase space for gluon emission due to the angular-ordering condition. Because of the presence of the Sudakov form factor in the KMR prescription, only the last emission generates transverse momentum of incoming gluons. This scheme is the direct analogy to the techniques usually applied in all standard parton shower Monte Carlo generators. The unique feature of the KMR model of UGDF is that it provides the possibility for the emission of at most one additional gluon. Therefore, one can expect that the KMR model may include in an effective way NLO corrections to the heavy quark production cross section.

In the literature, often somewhat differently defined UGDFs are used. They differ by the following transformation:

$$\mathcal{F}_g(x,k_t^2,\mu^2) \equiv \frac{1}{k_t^2}f_g(x,k_t^2,\mu^2). \tag{2.6}$$

The normalization condition for unintegrated distributions

$$g(x,\mu^2) = \int_0^{\mu^2} dk_t^2 f_g(x,k_t^2,\mu^2) \tag{2.7}$$

is exactly satisfied if we define

$$\frac{1}{k_t^2}f_g(x,k_t^2,\mu^2)|_{k_t<\mu_0} = \frac{1}{\mu_0^2}g(x,\mu_0^2)T_g(\mu_0^2,\mu^2), \tag{2.8}$$

so that the density of gluons in the proton is constant for $k_t < \mu_0$ at fixed x and μ.

The precise expression for the unintegrated gluon distribution reads

$$f_g(x,k_t^2,\mu^2) = T_g(k_t^2,\mu^2)\frac{\alpha_S(k_t^2)}{2\pi} \times \int_x^1 dz\left[\sum_q P_{gq}(z)\frac{x}{z}q\left(\frac{x}{z},k_t^2\right) + P_{gg}(z)\frac{x}{z}g\left(\frac{x}{z},k_t^2\right)\Theta\left(\frac{\mu}{\mu+k_t}-z\right)\right]. \tag{2.9}$$

III. APPLICATIONS OF k_t-FACTORIZATION

The k_t-factorization can be used to describe many high-energy processes. In this sense it is an alternative to the standard collinear-factorization approach. In the past, it was used for description of the deep-inelastic structure function [10,13,15], hadroproduction [4–11] and photoproduction [29,30] of heavy quarks, production of dijets in photoproduction [31] and deep-inelastic scattering [12], production of dijets in hadronic collisions [32–36], and electroweak boson production [37].

It is customary to describe first the F_2 proton structure function [10,13,15] and then use unintegrated gluon distributions to other processes. Almost all of the unintegrated parton distributions used here were tested in inclusive charm and associated charm and jet photoproduction at HERA (see, e.g., [30,31]).

It is very interesting and important to test them also in hadronic reactions. In the present paper, we concentrate on charm production in proton-proton scattering at the LHC. As discussed in our paper, here one enters a quite new kinematical and dynamical domain. Other processes, such as low transverse momentum dijet production, can be important, too. Complete off-shell matrix elements were derived only relatively recently in [38]. The calculation done in [32,34] used approximate matrix elements. An analysis of the dijet production at the LHC with a complete matrix element would be very interesting, too. This will be a subject of our future studies.

IV. CHARM QUARK AND ANTIQUARK PRODUCTION AT LHC

In this section, we concentrate on the production of charm quarks and antiquarks. Thus, this section has rather theoretical character. The cross sections for production of charmed mesons will be discussed in the next section. Before we go to the presentation of differential distributions, let us summarize integrated cross sections for $c\bar{c}$ production.

By using the KMR model of unintegrated gluon distributions, the total cross section for charm quark or antiquark production at $\sqrt{s} = 7$ TeV is obtained to be $\sigma_{\rm tot}^{\rm KMR}(pp \to c\bar{c}X) = 7.36^{+2.34}_{-1.77}(\mu)^{+6.03}_{-2.94}(m_c)$ mb. The predicted value has large uncertainties related to the choice of factorization or renormalization scales μ and due to the charm quark mass m_c. The obtained cross section is very large, of the same order as, e.g., the cross section for elastic scattering or single diffraction. This means that in practice charm quark or antiquarks appear in almost each inelastic event. This is a rather new situation which requires more detailed studies.

Taking into account acceptance of ATLAS, LHCb, and ALICE detectors, we get $\sigma_{\rm ATLAS}^{\rm KMR}(pp \to c\bar{c}X) = 2.53^{+0.83}_{-0.60}(\mu)^{+1.66}_{-0.90}(m_c)$ mb, $\sigma_{\rm LHCb}^{\rm KMR}(pp \to c\bar{c}X) = 1.54^{+0.50}_{-0.37}(\mu)^{+1.27}_{-0.62}(m_c)$ mb, and $\sigma_{\rm ALICE}^{\rm KMR}(pp \to c\bar{c}X) = 0.91^{+0.30}_{-0.23}(\mu)^{+0.68}_{-0.35}(m_c)$ mb, respectively. These numbers together with theoretical uncertainties are consistent with recent LHC measurements as well as with the recent FONLL [39] and general-mass variable-flavour-number scheme [40] predictions of the charm cross section.

As was mentioned in the previous section, our predictions are very sensitive to the choice of unintegrated gluon distributions. Different UGDFs are very often based on quite different theoretical assumptions. This has a crucial meaning for their kinematical characteristics. In Fig. 1, we show dependence of the unintegrated gluon distributions functions on gluon transverse momentum squared k_t^2 for several values of x relevant for the production of charm quarks and antiquarks at LHC energy. Differences in shapes in k_t^2 of the plotted functions are significant. One can also see different dependence on x of the different considered UGDFs. By changing the value of x, the mutual trends between them also change what makes the overall picture more complicated. Especially the KMR model seems to reveal the strongest x dependence.

The rapidity of the quark or antiquark is strongly correlated with longitudinal momentum fractions of gluons

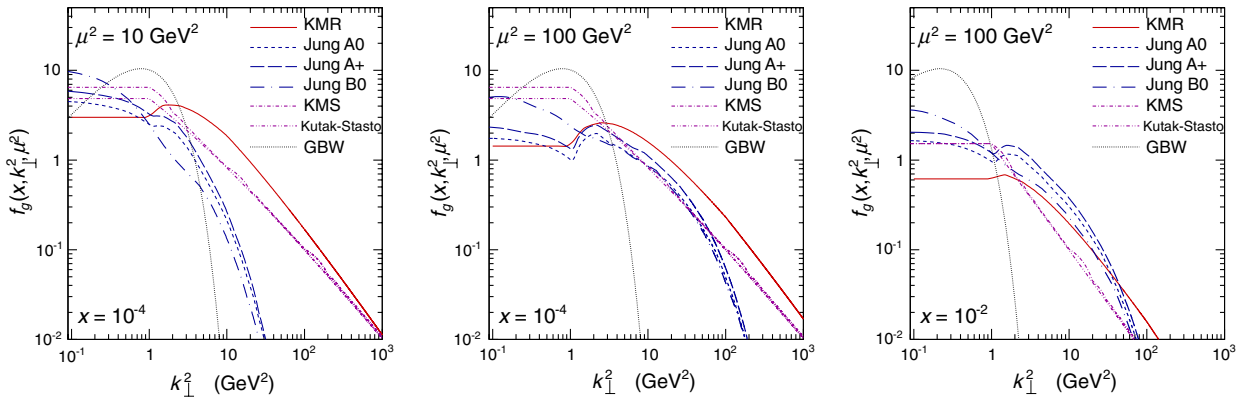

FIG. 1 (color online). Different unintegrated gluon distributions from the literature as a function of gluon transverse momentum squared k_t^2 for different values of longitudinal momentum fraction x of the gluon initiating the hard process and for different factorization scales μ.

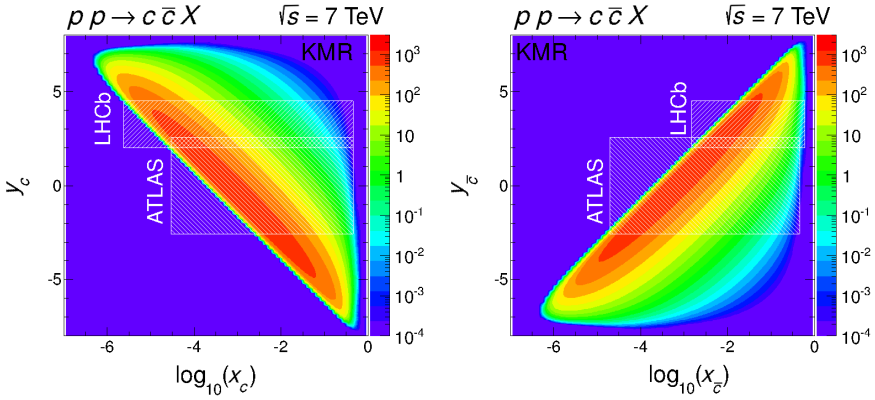

FIG. 2 (color online). The range of the longitudinal momentum fraction of gluons and its correlation to the rapidity of the charm quark (left) or antiquark (right). In addition, regions of the coverage for the ATLAS and LHCb experiments are shown.

initiating the hard process. This is shown in Fig. 2 for the KMR UGDF. At rapidities $|y| > 5$, one starts to probe longitudinal momentum fractions smaller than 10^{-4}. This is a new situation compared to earlier measurements at RHIC or Tevatron. The UGDFs as well as standard collinear ones (PDFs) were not tested so far in this region.

It was advocated in Ref. [41] that the two-dimensional distribution in transverse momentum of the charm quark and charm antiquark can be a good "theoretical observable" to study unintegrated gluon distributions. In Fig. 3, we show such distributions for different UGDFs from the literature. We use here KMR [12], Kwieciński-Martin-Staśto (KMS) [13], Kutak-Stasto [14], Jung setA+ and setB+ [15], and Golec-Biernat-Wüsthof (GBW) [16] parametrizations. Quite different patterns are obtained for different UGDFs. This may have direct consequences for correlation observables for mesons or/and nonphotonic electrons. Moreover, events when one p_t is small and the second one is large correspond to the region relevant for higher-order collinear corrections. It is clear from this

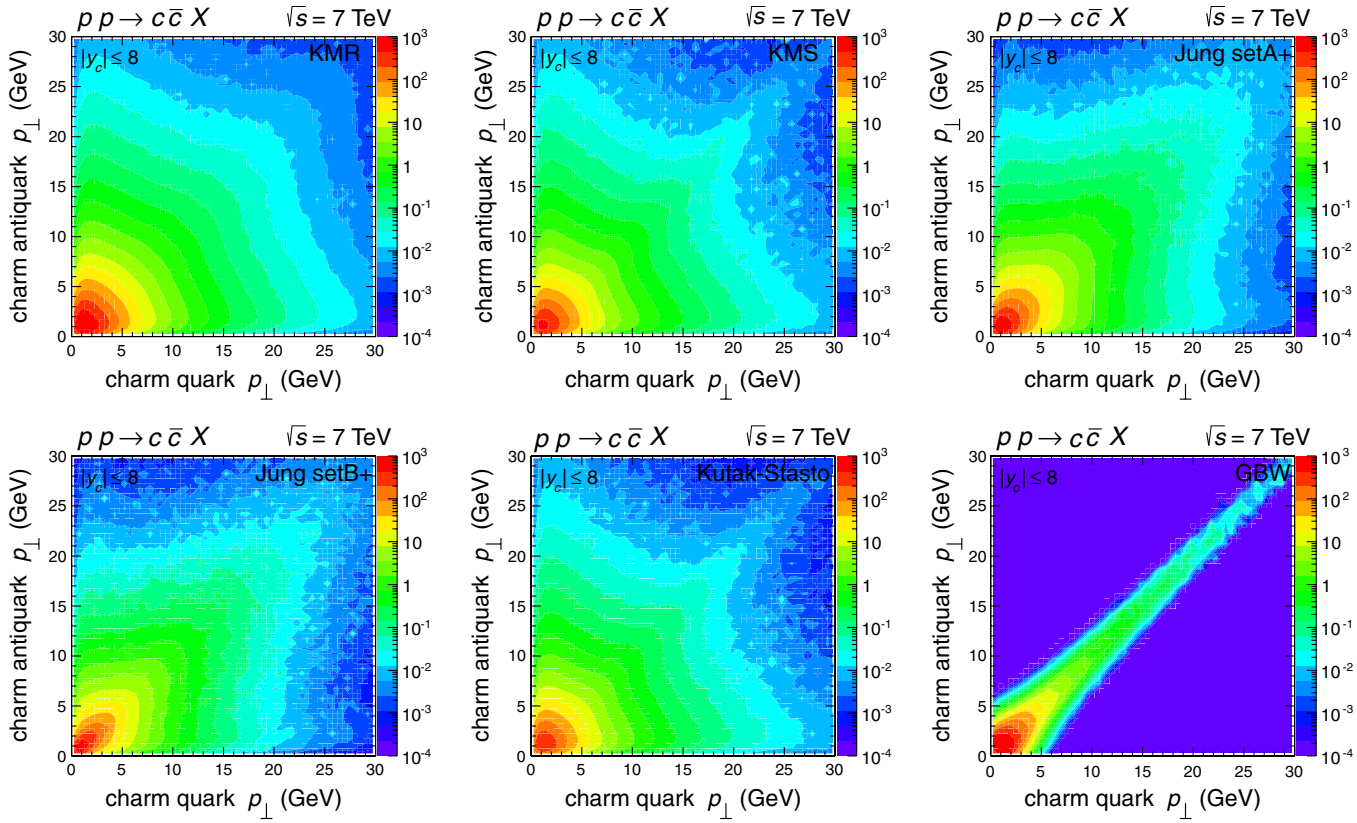

FIG. 3 (color online). Two-dimensional maps in the transverse momentum of the charm quark and transverse momentum of the charm antiquark for different unintegrated gluon distributions.

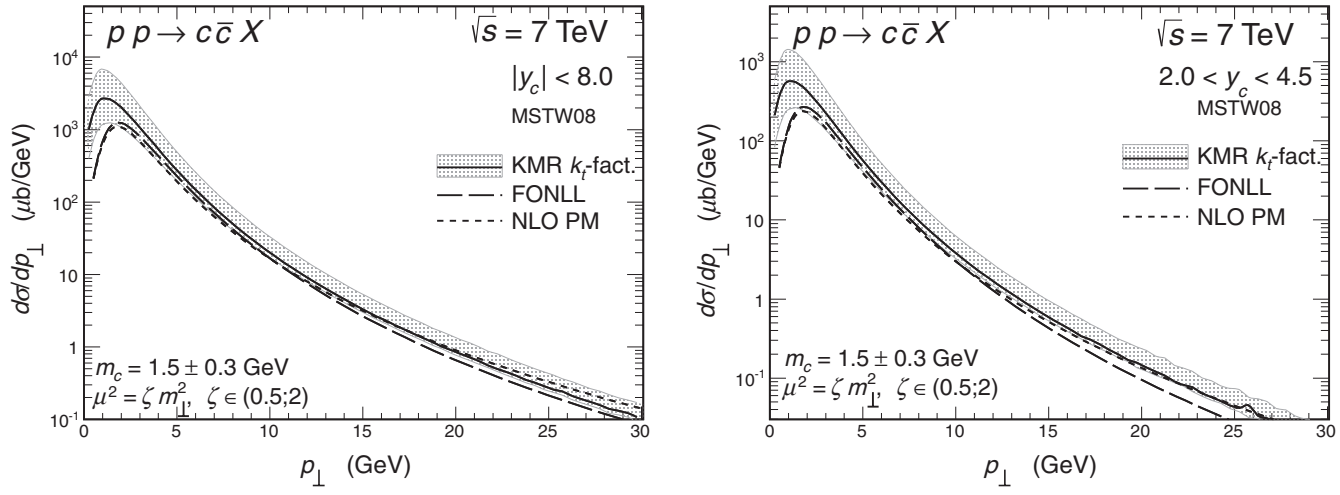

FIG. 4. Theoretical uncertainties on transverse momentum distribution of c or $\bar{c}$ production due to the choice of factorization or renormalization scale and those related to charm quark mass for the KMR UGDF (solid line with the shaded bands). The left panel shows the cross section for the whole range of quark or antiquark rapidities, while the left panel for the rapidity range relevant for the LHCb experiment. For comparison, the FONLL and NLO PM predictions are also shown.

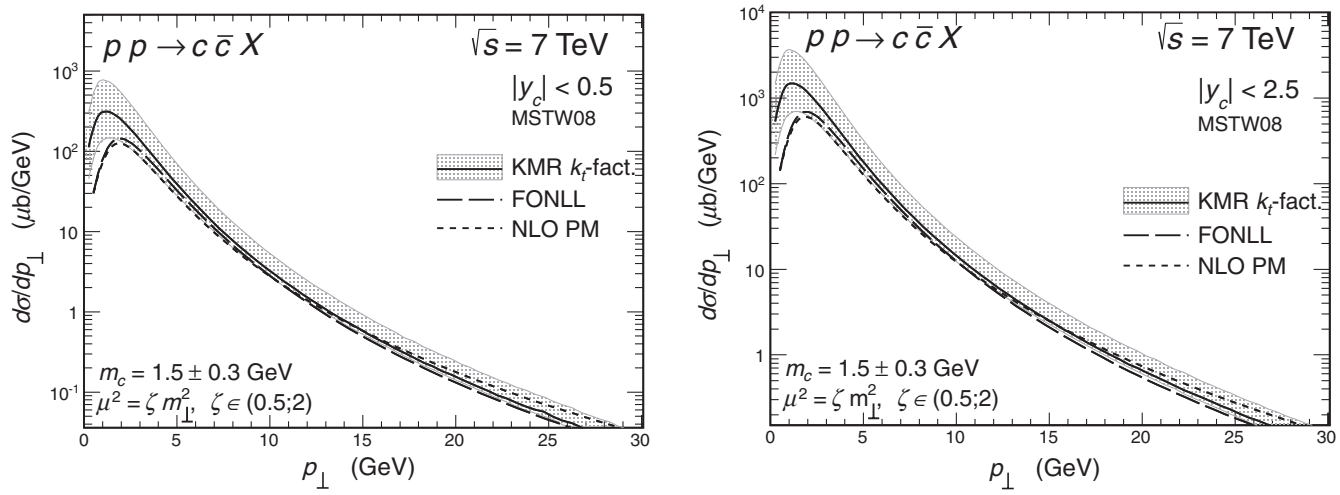

FIG. 5. The same as in Fig. 4 but for the ALICE (left panel) and ATLAS or CMS (right panel) kinematics.

$p_{1t}p_{2t}$ plane that effects of an effective inclusion of NLO diagrams in the k_t-factorization approach strongly depend on the construction of UGDFs.

The production of charmed mesons strongly depends on the choice of UGDF model as will be discussed in the next section. As will become clear, there the KMR UGDF within rather large theoretical uncertainties provides the best description of the LHC experimental data. The major part of these uncertainties comes from the perturbative part of the calculation. Therefore, in the following, we spend some time to define uncertainties of the corresponding calculations at the quark level. In Figs. 4 and 5, we present the uncertainties of our predictions, obtained by changing charm quark mass $m_c = 1.5 \pm 0.3$ GeV and by varying renormalization and factorization scales $\mu^2 = \zeta m_t^2$, where $\zeta \in (0.5; 2)$. The gray shaded bands represent both these sources of uncertainties summed in quadrature. The smaller the transverse momentum, the larger the uncertainty. For comparison, we show also results for the FONLL [2] and fixed-order NLO (denoted in figures as NLO PM) approaches. Our result of the k_t-factorization approach is consistent within the uncertainty bands with those rather standard NLO collinear calculations. Only at small quark p_t's does some difference appear. This is the region where transverse momenta of incident gluons play an important role. Particularly, a detailed treatment of the nonperturbative k_t region in UGDF may lead to a dumping or an enhancement of the cross section at small p_t.

V. PRODUCTION OF CHARMED MESONS

The hadronization of heavy quarks is usually done with the help of fragmentation functions. The inclusive

TABLE I. Integrated cross sections for production of different D mesons at the LHC.

Acceptance	Mode	$\sigma_{\rm tot}^{\rm EXP}$ [μb]	$\sigma_{\rm tot}^{\rm THEORY}$ [μb] KMR$^{+}_{-}(\mu)^{+}_{-}(m_c)$	Jung setA0+	KMS
ALICE	$(D^0+\bar{D}^0)/2$	$516 \pm 41^{+69}_{-175}$	$514^{+169\ +384}_{-130\ -198}$	317	313
$\lvert y\rvert < 0.5$	$(D^+ + D^-)/2$	$248 \pm 30^{+52}_{-92}$	$206^{+68\ +154}_{-52\ -79}$	127	125
	$(D^{*+} + D^{*-})/2$	$247 \pm 27^{+36}_{-81}$	$208^{+69\ +156}_{-53\ -80}$	129	127
ALICE $\lvert y\rvert < 0.5$ $2 < p_\perp < 12$ GeV	$(D_S^+ + D_S^-)/2$	$53 \pm 12^{+13}_{-15}$	$20^{+5\ +7(+20\%)}_{-4\ -5}$	$13^{(+20\%)}$	$13^{(+20\%)}$
LHCb	$D^0+\bar{D}^0$	1488 ± 182	$1744^{+565\ +1435}_{-418\ -700}$	1162	872
$2 < y < 4.5$	$D^+ + D^-$	717 ± 109	$697^{+226\ +574}_{-167\ -280}$	465	349
$0 < p_\perp < 8$ GeV	$D^{*+} + D^{*-}$	676 ± 137	$705^{+229\ +582}_{-169\ -284}$	471	354
	$D_S^+ + D_S^-$	194 ± 38	$246^{+80\ +203}_{-59\ -99}$	164	123
ATLAS	$D^+ + D^-$	$238 \pm 13^{+35}_{-23}$	$137^{+31\ +30(+20\%)}_{-20\ -24}$	$103^{(+20\%)}$	$93^{(+20\%)}$
$\lvert\eta\rvert < 2.1$	$D_S^+ + D_S^-$	$168 \pm 34^{+27}_{-25}$	$48^{+12\ +11(+20\%)}_{-7\ -8}$	$36^{(+20\%)}$	$33^{(+20\%)}$
$p_\perp > 3.5$ GeV	$D^{*+} + D^{*-}$	$285 \pm 16^{+32}_{-27}$	$155^{+37\ +37(+20\%)}_{-22\ -28}$	$115^{(+20\%)}$	$104^{(+20\%)}$

distributions of charmed mesons can be obtained through a convolution of inclusive distributions of charm quarks or antiquarks and $c \to D$ fragmentation functions:

$$\frac{d\sigma(pp\to D\bar{D}X)}{dy_D d^2p_{t,D}} \approx \int_0^1 \frac{dz}{z^2} D_{c\to D}(z) \frac{d\sigma(pp\to c\bar{c}X)}{dy_c d^2p_{t,c}}\Big|_{\substack{y_c=y_D \\ p_{t,c}=p_{t,D}/z}}, \tag{5.1}$$

where $p_{t,c} = \frac{p_{t,D}}{z}$ and z is the fraction of longitudinal momentum of the heavy quark carried by the meson. We have made a typical approximation assuming that y_c is unchanged in the fragmentation process, i.e., $y_D = y_c$.

As a default set in our calculations, we use the standard Peterson model of fragmentation function [42] with the parameter $\varepsilon_c = 0.05$. This value was extracted by ZEUS and H1 analyses and seems to be relevant for LO calculations. However, in the fragmentation scheme applied in the FONLL framework, rather harder functions (or smaller ε_c) are suggested [43]. This issue together with effects of applying other fragmentation functions from the literature [44–46] will be discussed in more detail when discussing differential distributions. The fragmentation functions used here are normalized to branching fractions from [47].

For the production of light mesons (pions and kaons), evolution of fragmentation functions is included routinely. For heavy mesons (D or B), usually the evolution is neglected. This is done in all k_t-factorization applications as well as in FONLL. How important is the QCD evolution was discussed only by Kniehl *et al.* [48]. The most recent work of the group can be found in [49]. There, they have determined nonperturbative fragmentation functions for D^0, D^+, and D^* mesons by fitting the Belle, CLEO, ALEPH, and OPAL Collaboration data including DGLAP evolution. We shall show D meson transverse momentum distributions for these more modern fragmentation functions.

In Table I, we have collected integrated cross sections for the production of different species of D mesons. Measured cross sections from different LHC experiments are compared to theoretical predictions obtained with three sets of UGDFs. The error bars shown for the KMR UGDF reflect uncertainty due to the choice of factorization or renormalization scale (μ) and related to the mass of the quark (m_c). The fractional uncertainties due to both these sources for other UGDFs are similar. Only cross sections obtained with the KMR UGDF are consistent within error bars with the experimental data.

In the cases of measurements with the full coverage of the meson transverse momentum range, the theoretical cross sections are almost insensitive to the fragmentation model. A quite different situation is observed when the small p_t region is excluded. In the latter case, using the Peterson model with $\varepsilon_c = 0.02$ (which gives results closer to the FONLL predictions) we note the enhancement of the integrated cross sections by about 20%.

Let us start the presentation of differential distributions for different LHC experiments.

A. ALICE

Let us focus first on the production of charmed mesons at midrapidities. The ALICE Collaboration has performed a measurement of the transverse momentum distribution of D^0, D^+, D^{*+}, and D_s^+ [20,21]. In the very limited range of (pseudo)rapidity, one tests unintegrated gluon distributions in a pretty narrow region of longitudinal momentum fractions (see Fig. 2). In Fig. 6, we show the transverse momentum distribution of D^0 mesons. In the left panel, we present results for different UGDFs known from the

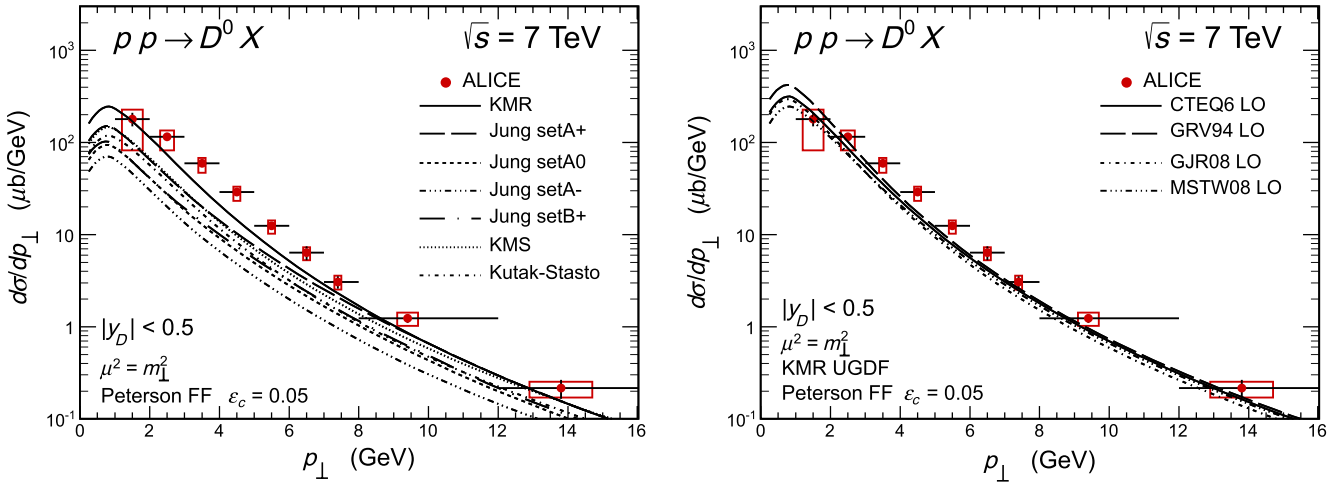

FIG. 6 (color online). Transverse momentum distribution of D^0 mesons for the ALICE measurement. The left panel shows results for different UGDFs, while the right panel shows uncertainties due to the choice of collinear gluon distributions in the calculation of the KMR UGDF.

literature. Most of the existing distributions fail to describe the ALICE data. The KMR UGDF provides the best description of the measured distributions. Therefore, in the following, we shall concentrate on the results obtained with the KMR UGDF. In the right panel, we show uncertainties due to the choice of usual integrated collinear gluon distributions (PDFs) used for calculating the KMR UGDF. In the latter case, the biggest uncertainty can be observed at small transverse momenta, i.e., in the region of the small gluon longitudinal momentum fraction. We use rather up-to-date MSTW08 [50], CTEQ6 [51], and GJR08 [52] parametrizations as well as GRV94 [53], which is fairly old but was very often used in the past years in similar analyses. For more detailed discussion of the PDF aspects in charm production, we refer the reader to Ref. [54]. In Fig. 7, we show separately uncertainties due to the choice of factorization or renormalization scale (left panel) and those due to the choice of the quark mass (right panel). The uncertainties due to the choice of scales are rather large. The uncertainties due to quark mass are significant only at small transverse momenta. They are calculated by varying the quark mass $m_c = 1.5 \pm 0.3$ GeV and are representative for all other UGDFs.

In Figs. 8 and 9, we present corresponding plots for D^+ mesons. The situation here is very similar to the case of D^0 mesons.

Let us quantify now uncertainties due to the fragmentation process. Figure 10 shows results for D^0 (left panel) and D^+ (right panel) mesons for different fragmentation functions from the literature. We use here the Peterson model with three different sets of the ε_c parameter, as well as Braaten *et al.* [44], Kartvelishvili *et al.* [45], and Collins-Spiller [46] parametrizations. All of the applied functions give similar results. The effects related to the fragmentation

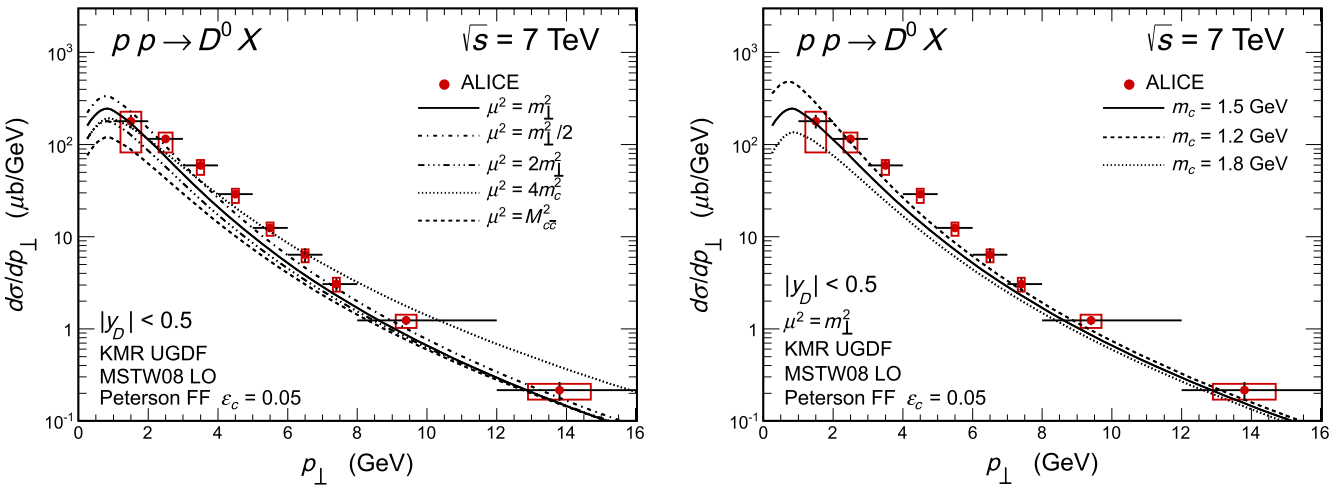

FIG. 7 (color online). Uncertainties of the theoretical cross section for the D^0 meson production within the ALICE acceptance due to the choice of the scale (left) and due to the quark mass (right).

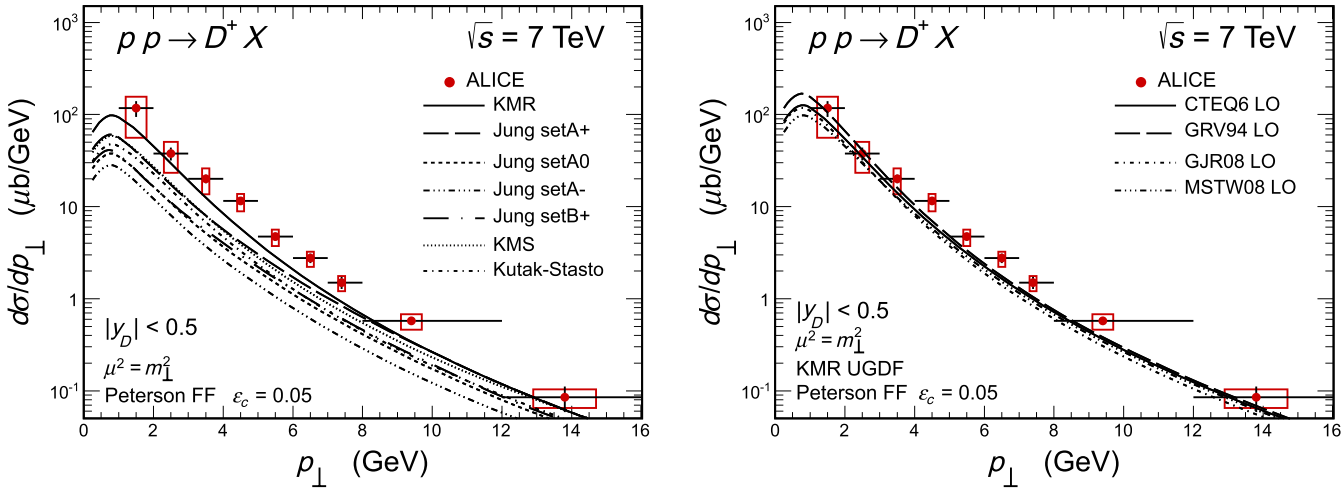

FIG. 8 (color online). The same as in Fig. 6 but for the production of D^+ mesons.

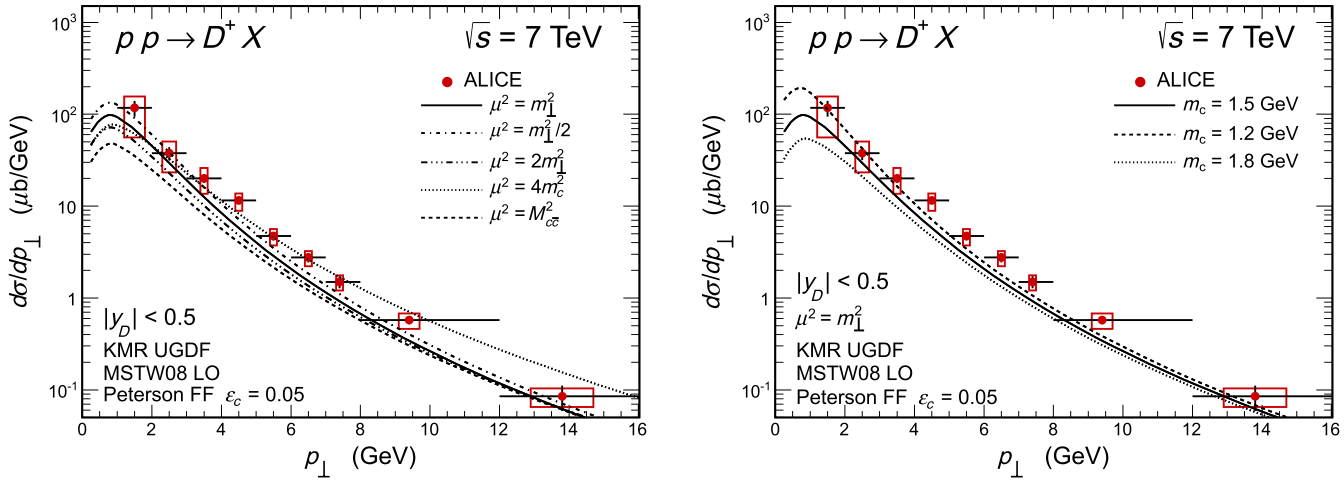

FIG. 9 (color online). The same as in Fig. 7 but for the D^+ meson.

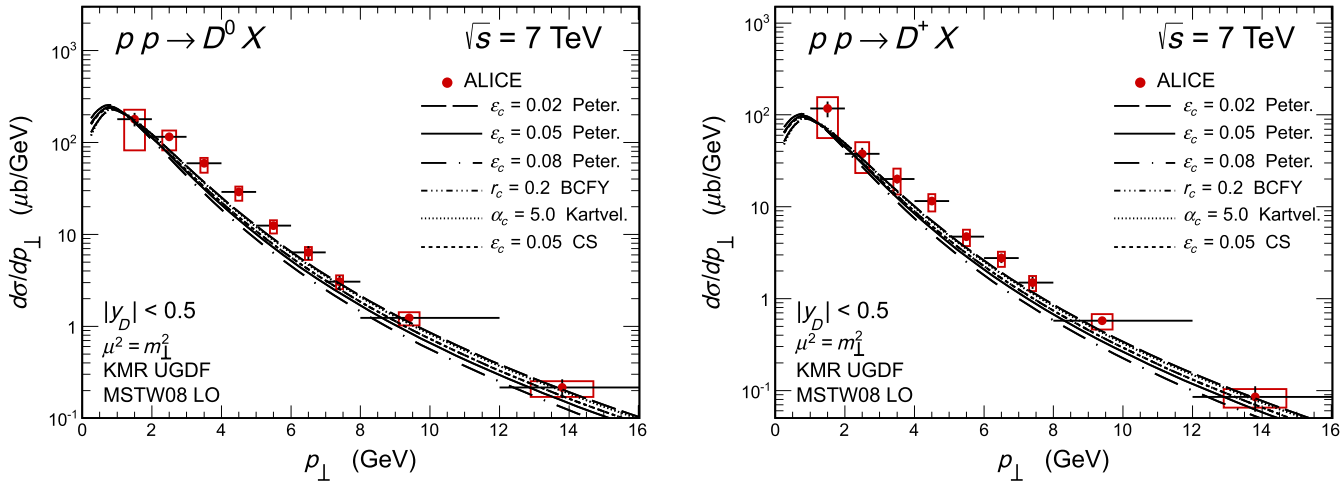

FIG. 10 (color online). Uncertainties due to fragmentation parameter ε_c in the Peterson fragmentation function and related to the choice of other fragmentation models for the KMR UGDFs.

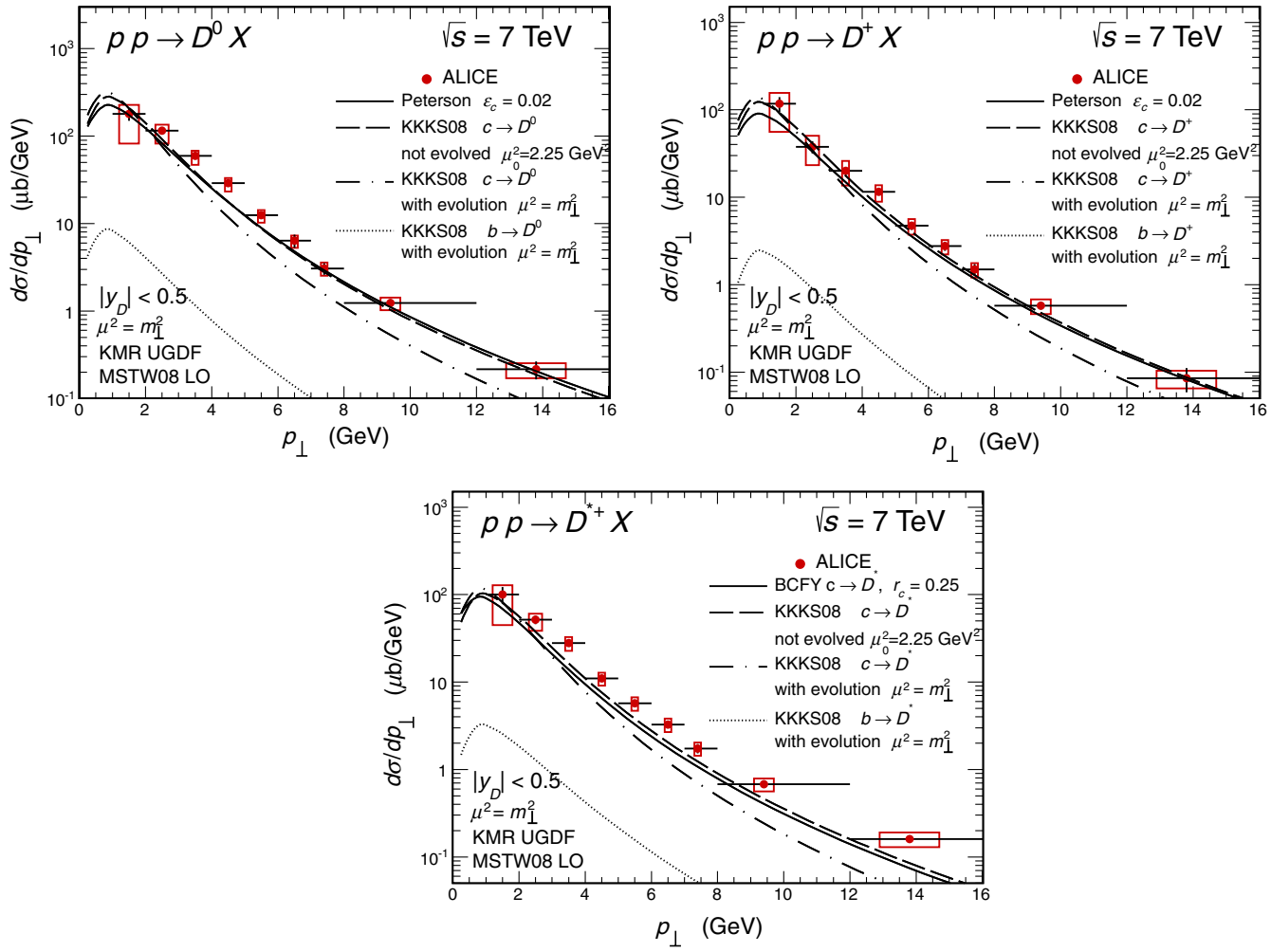

FIG. 11 (color online). Effect of the evolution of the fragmentation functions for D^0, D^+, and D^* for the ALICE kinematics. We compare results obtained with the KKKS08 fragmentation function with the other commonly used functions. The $b \to D$ contribution is shown in addition. The details are specified in the figures.

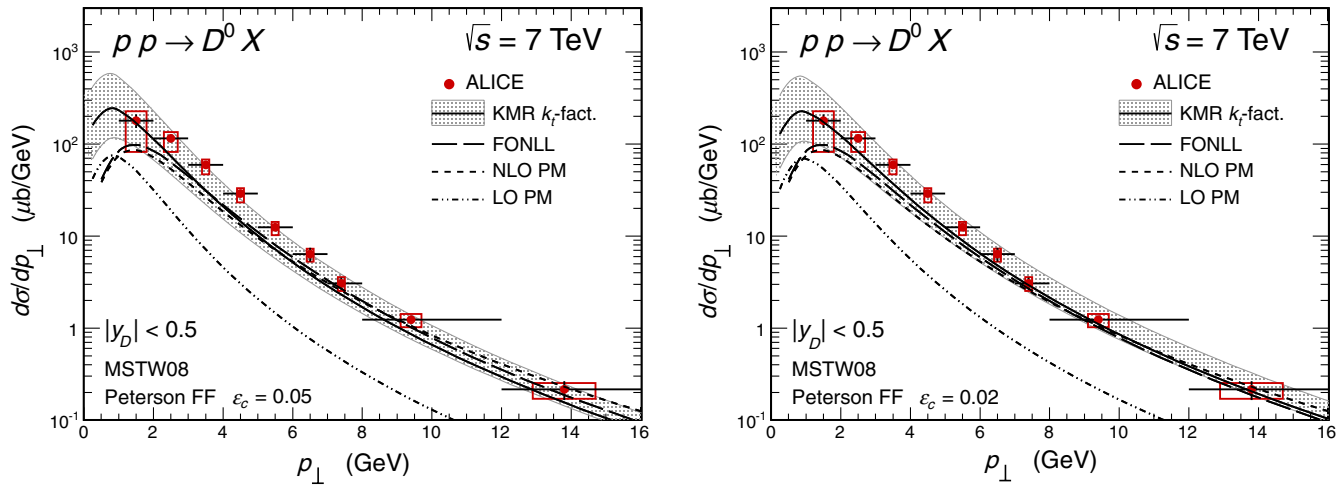

FIG. 12 (color online). Transverse momentum distribution of D^0 mesons for the ALICE kinematical region for different values of the Peterson ε_c parameter. Together with our predictions for the KMR UGDF (solid line with shaded band), results of different popular approaches are also shown.

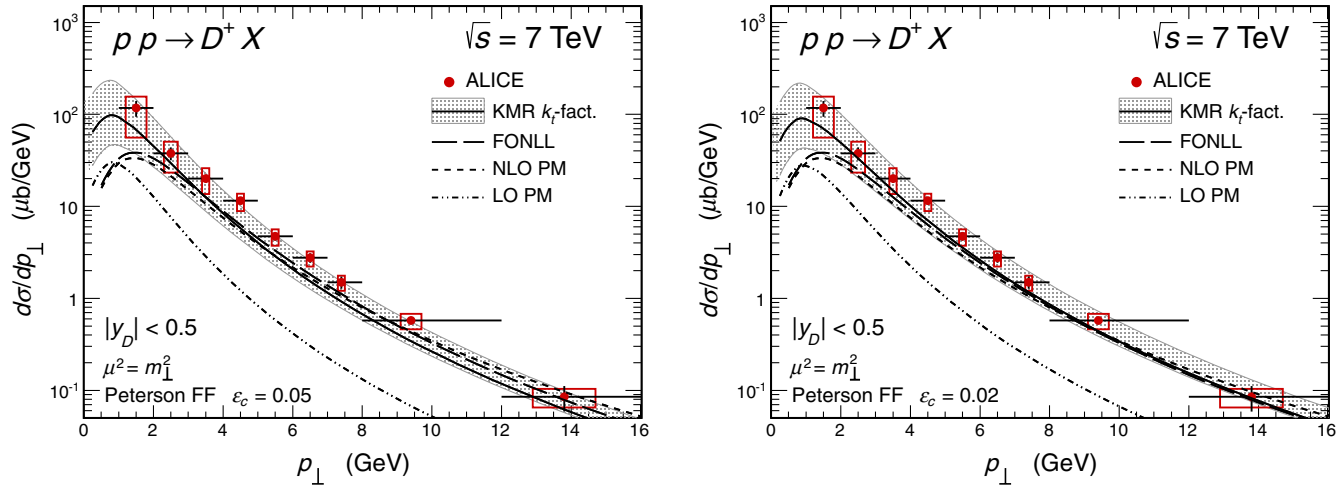

FIG. 13 (color online). The same as in Fig. 12 but for the D^+ meson.

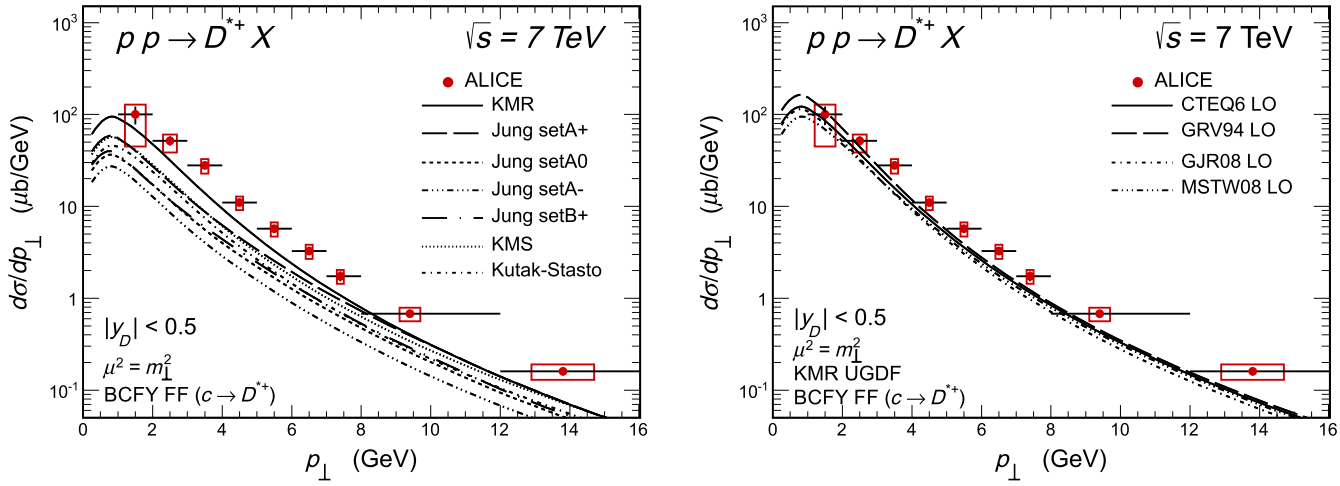

FIG. 14 (color online). Transverse momentum distribution of D^{*+} mesons for different UGDFs (left) and the uncertainties due to the choice of collinear PDFs used in calculating the KMR UGDF (right).

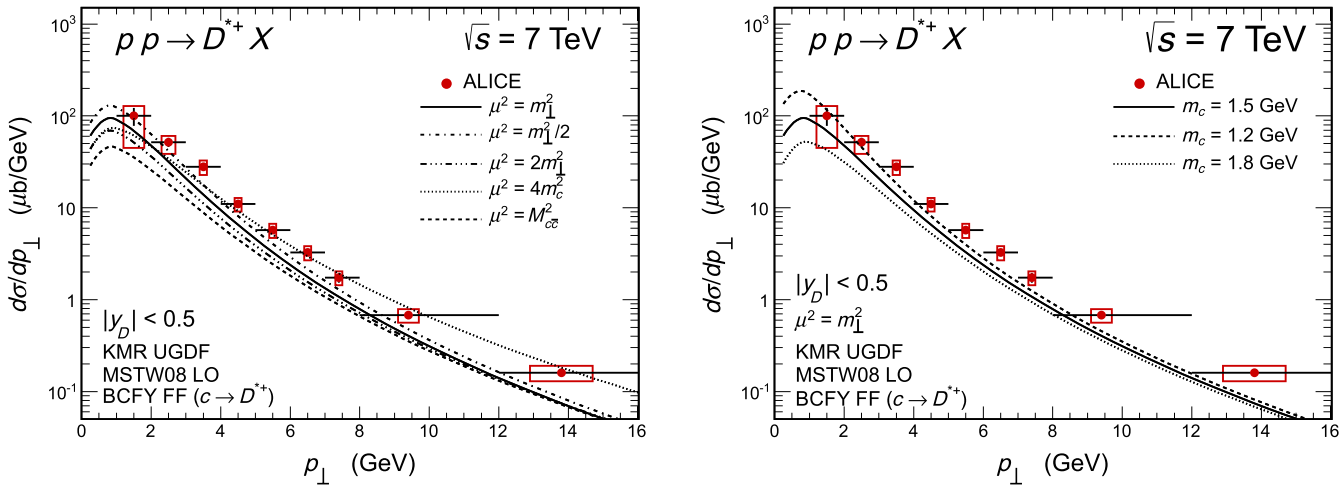

FIG. 15 (color online). Transverse momentum distribution of D^{*+} mesons. Shown are uncertainties due to the choice of scales in the KMR UGDF (left panel) and due to the quark masses (right panel).

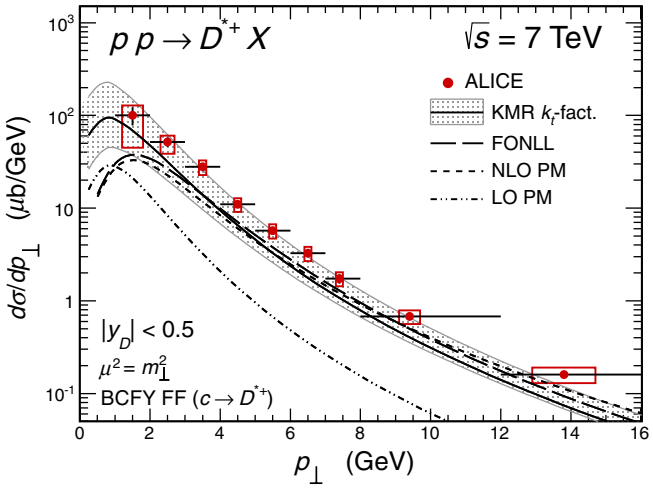

FIG. 16 (color online). Transverse momentum distribution of D^{*+} mesons for different approaches known from the literature. The gray band represents overall uncertainties of the k_t-factorization approach with the KMR UGDF.

process seem to be important only at larger meson p_t's, starting from $p_t = 3$ GeV.

In Fig. 11, we show also results with the Kneesch-Kramer-Kniehl-Schienbein (KKKS08) fragmentation function [49] which includes QCD evolution. We take $\mu^2 = m_\perp^2$ (quark transverse mass squared) as the running scale of the evolution. Smaller cross sections for large transverse momenta are obtained (long dashed-dotted line). For illustration, we show also the result when the evolution is neglected. The corresponding result is almost the same as for the Peterson fragmentation function. The contribution for $b \to D$ fragmentation is shown separately.

Let us compare now results of our approach to the results of some other popular approaches used in the literature. In Figs. 12 and 13, we present such a comparison. Our results obtained within the k_t-factorization approach with the KMR UGDF are very similar to those obtained within NLO PM and FONLL models. The cross sections obtained within the leading-order collinear approximation (LO PM) are much smaller, in particular for larger transverse momenta. Comparing the left and right panels of these figures, one can observe an improvement of the large p_t data description when $\varepsilon_c = 0.02$ in the Peterson function is taken. This choice corresponds to the upper limit of our uncertainties in the hadronization. It makes our results closer to those from FONLL. In the FONLL approach, as a default fragmentation scheme for charm quarks the Braaten-Cheung-Fleming-Yuan (BCFY) model with $r_c = 0.1$ is used. However, the Peterson parametrization with $\varepsilon_c = 0.02$ gives, in general, very similar characteristics. Since our k_t-factorization calculation is very similar to the FONLL predictions at the quark level (see Fig. 5), application of the harder fragmentation functions may be justified.

Now let us consider for the moment distributions for vector mesons D^{*+}. In Fig. 14, we show transverse momentum distributions of D^{*+} for different UGDFs and uncertainties in calculating distributions with the KMR UGDF due to the choice of collinear gluon distributions. As in the previous cases, the choice of collinear PDFs has some importance only at small transverse momenta. The same conclusions as in the cases of pseudoscalar mesons come from Fig. 15, where uncertainties due to the scales (left) and related to the quark mass (right) are presented. In Fig. 16, both of these sources are taken together, and our predictions with the KMR UGDF are confronted once again with LO and NLO PM collinear calculations. Here we use the Braaten *et al.* model for fragmentation which has parametrization of the fragmentation function for the transition of a heavy quark into a vector meson state.

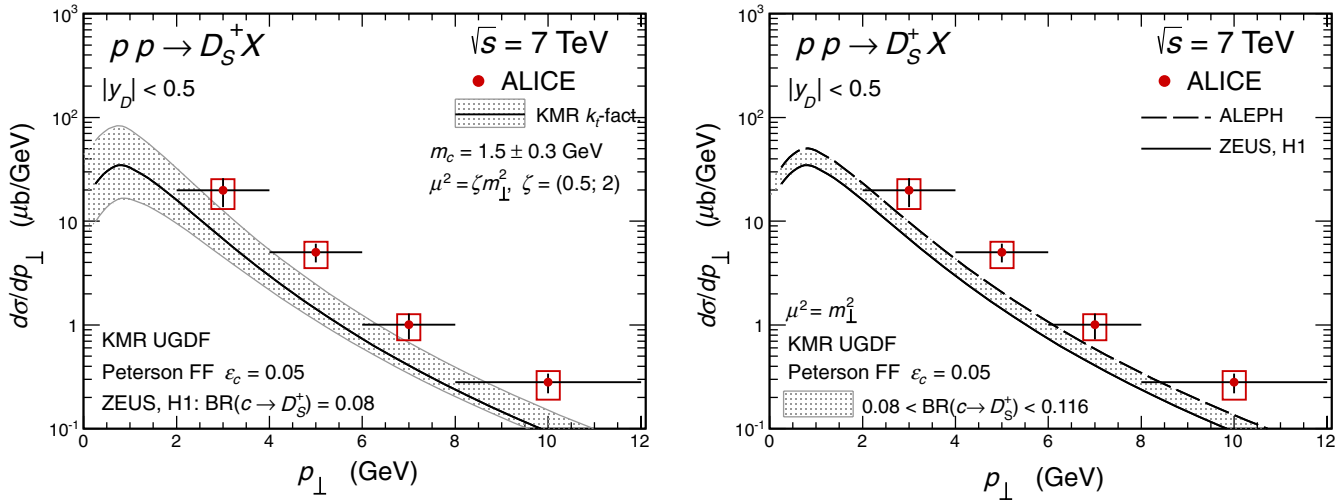

FIG. 17 (color online). Transverse momentum distribution of D_s^+ mesons. We show uncertainties due to the choice of scales and masses (left panel) and uncertainties related to poorly known fragmentation branching fraction BR($c \to D_S^+$) (right panel).

Finally, in Fig. 17, we show distributions for D_s^+ mesons, i.e., mesons built of charm and strange quarks or antiquarks. The corresponding cross section is considerably smaller than for the charm mesons containing light (up or down) quarks or antiquarks. The general situation is, however, very similar. The KMR UGDF provides the best agreement with the ALICE data. Results for other UGDFs are much below the experimental data which means, in our opinion, that they do not pass the powerful test. In the case of the D_S^+ meson, a different, quite important source of uncertainties appears, namely, the poorly known fragmentation fractions $\mathrm{BR}(c \to D_S^+)$. By changing the value from 0.08 (ZEUS and H1) to 0.116 (ALEPH), a significant enhancement of the theoretical predictions is achieved.

B. ATLAS

The ATLAS experiment covers much broader range of pseudorapidities than ALICE. As a consequence, one tests broader region of longitudinal momentum fractions $10^{-4} < x_1,\ x_2 < 10^{-2}$. The gluon distributions in this range of x_1 and x_2 values carried by gluons are rather well known. Also, application of the known UGDFs from the literature should be reliable.

Figure 18 shows transverse momentum distributions of charged pseudoscalar $D^\pm$ mesons for different models of unintegrated distributions, for $\varepsilon_c = 0.05$ (left) and $\varepsilon_c = 0.02$ (right). The general situation is very similar as for the ALICE experiment, although the agreement is somewhat worse. Only the upper limit of the KMR result is compatible with the ATLAS experimental data. This may be caused by a much broader range of pseudorapidities in the case of the ATLAS detector. Potentially, this can be related to double-parton scattering effects to be discussed elsewhere [55]. Also, the other standard approaches give results below the ATLAS data as can be seen in Fig. 19.

Because of the fairly large span of pseudorapidities, the ATLAS Collaboration can extract also pseudorapidity

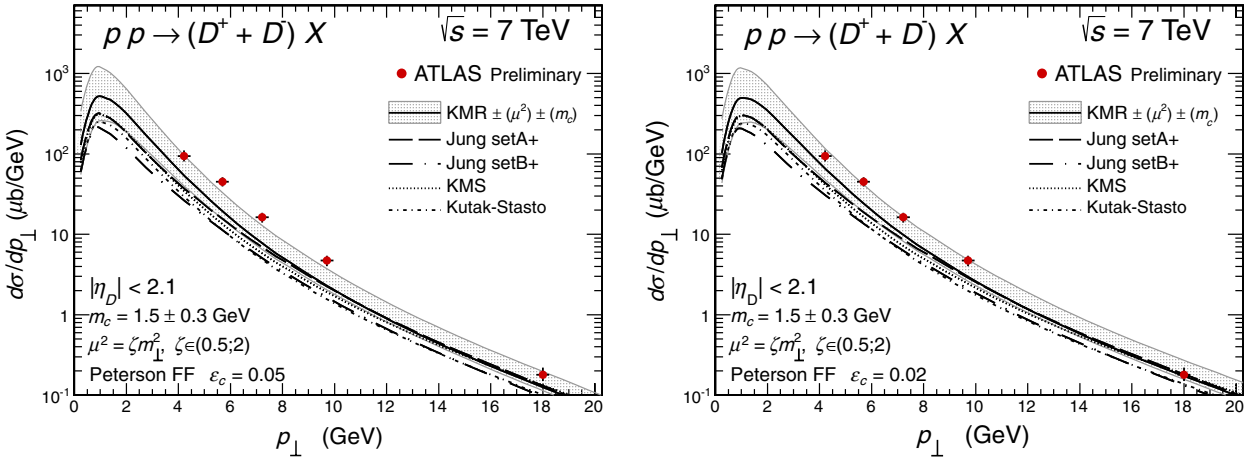

FIG. 18 (color online). Transverse momentum distribution of $D^\pm$ mesons for different UGDFs from the literature compared with the preliminary ATLAS experimental data for $\varepsilon_c = 0.05$ (left) and $\varepsilon_c = 0.02$ (right).

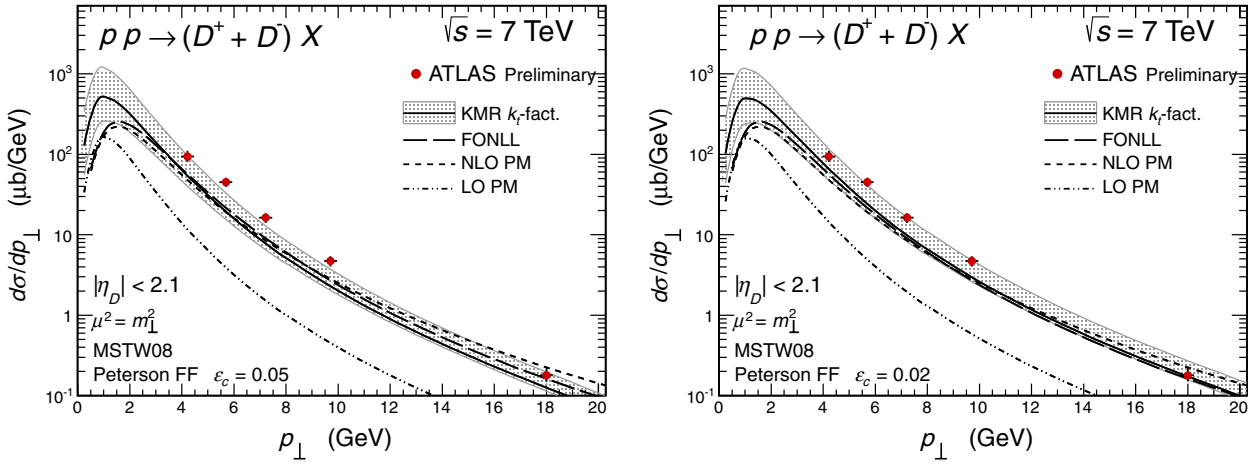

FIG. 19 (color online). Transverse momentum distribution of $D^\pm$ mesons for different standard approaches compared with the ATLAS experimental data [19] for $\varepsilon_c = 0.05$ (left) and $\varepsilon_c = 0.02$ (right). The details are specified in the figures.

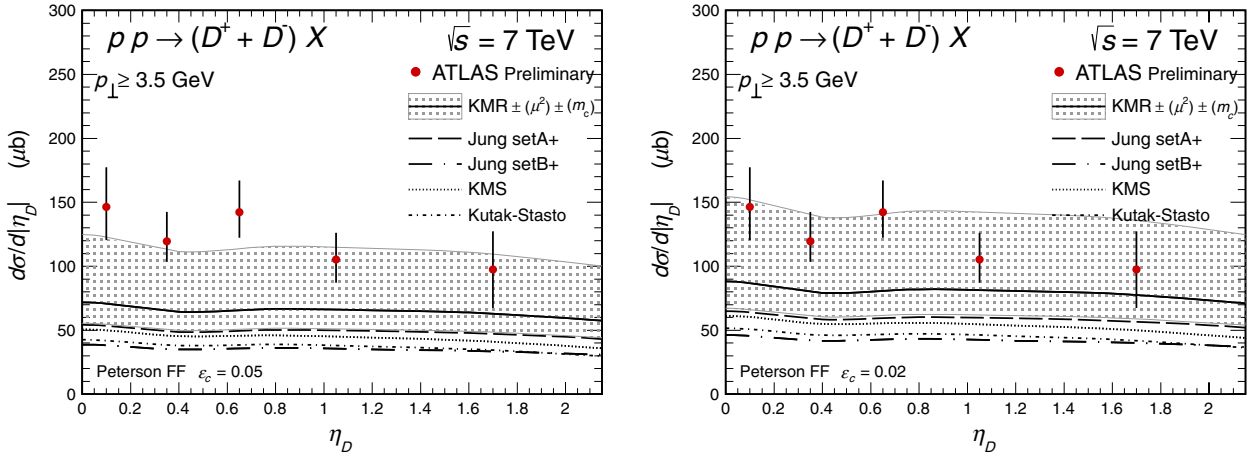

FIG. 20 (color online). Distribution in $D^\pm$ meson pseudorapidity. The results for different UGDFs are compared with the ATLAS preliminary data [19] for different values of the parameter ε_c of the Peterson fragmentation function: $\varepsilon_c = 0.05$ (left) and $\varepsilon_c = 0.02$ (right).

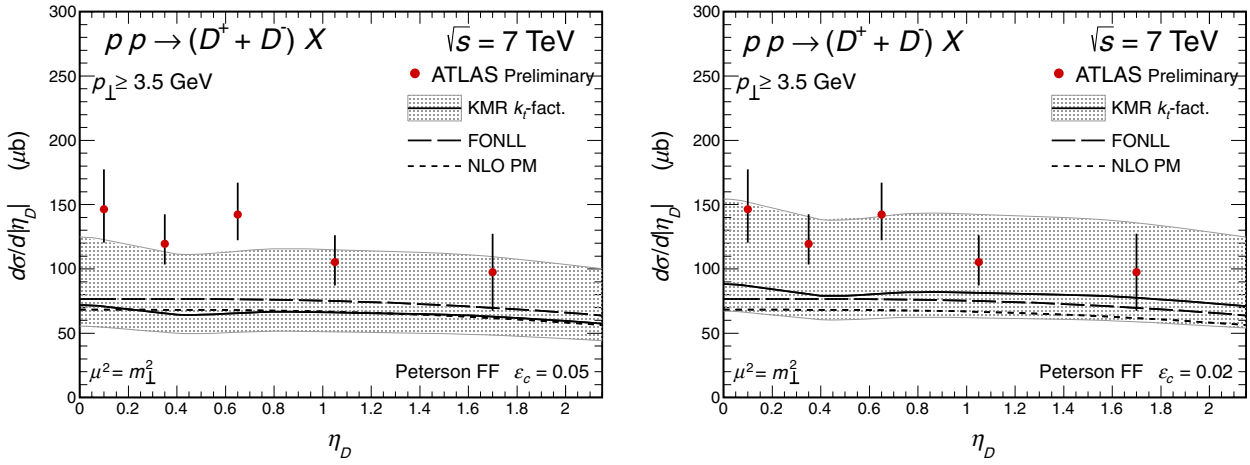

FIG. 21 (color online). Distribution in $D^\pm$ meson pseudorapidity. The results of our calculation are compared with those for other calculations and with the ATLAS preliminary data [19] for different values of the parameter ε_c of the Peterson fragmentation function: $\varepsilon_c = 0.05$ (left) and $\varepsilon_c = 0.02$ (right).

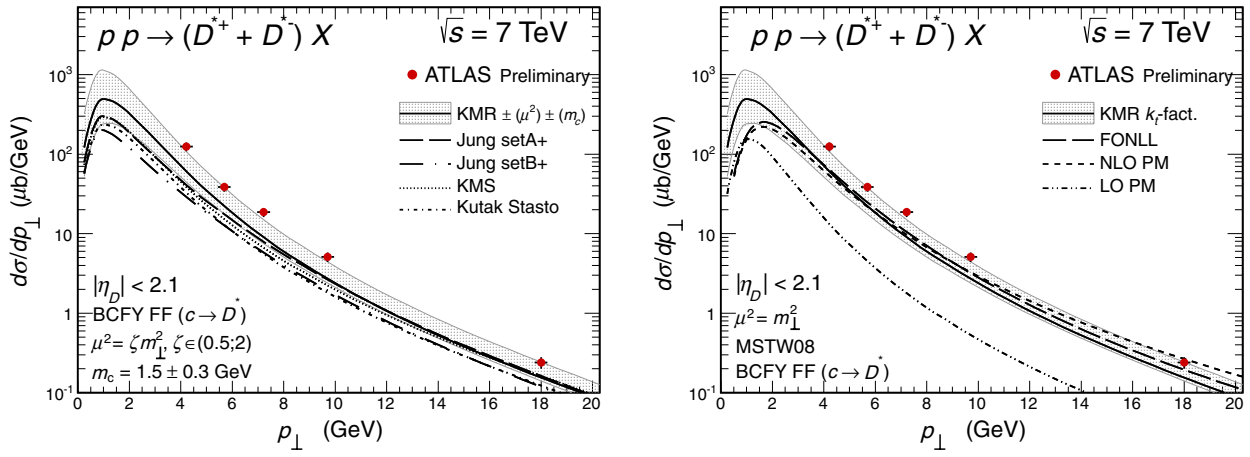

FIG. 22 (color online). Distribution in D^{*+} meson transverse momentum. The results of our calculation are compared with the ATLAS preliminary data [19]. In the left panel we show results for different UGDFs, and in the right panel our results are compared with other approaches.

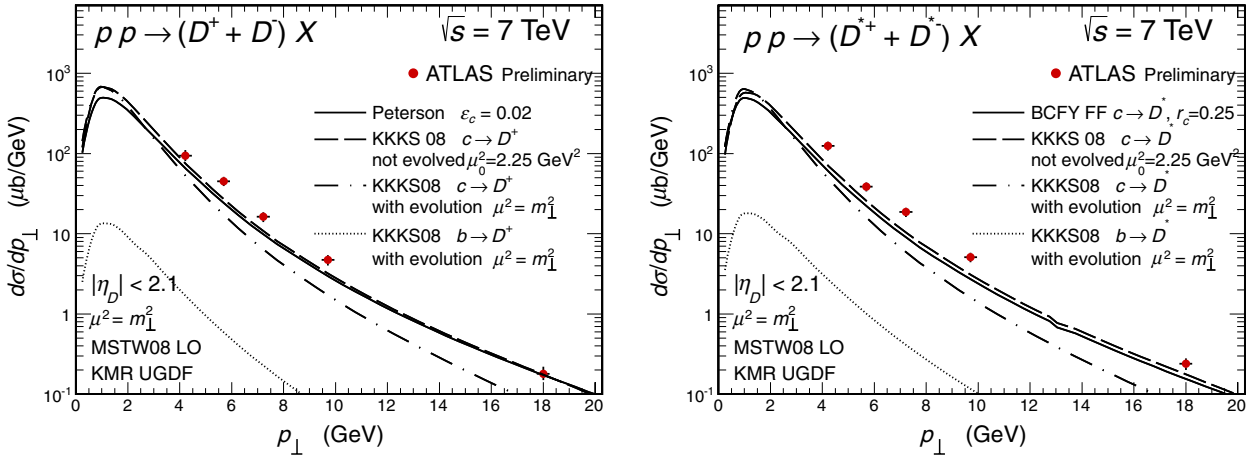

FIG. 23 (color online). Effect of the evolution of the fragmentation functions for D^+ and D^* for the ATLAS kinematics. We compare results obtained with the KKKS08 fragmentation function with the other commonly used functions. The $b \to D$ contribution is shown in addition. The details are specified in the figures.

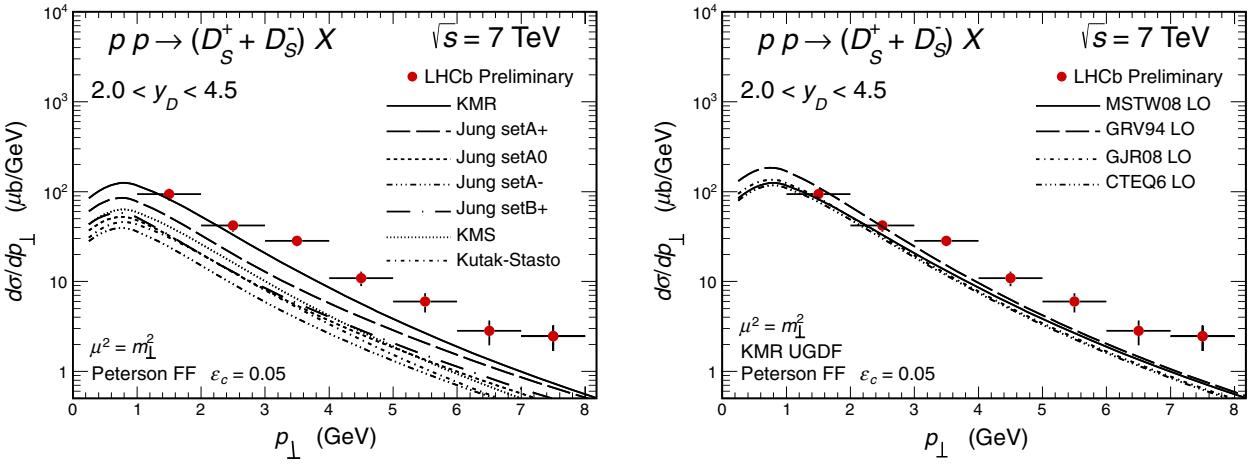

FIG. 24 (color online). Transverse momentum distribution of $D_s^{\pm}$ mesons for different UGDFs from the literature (left) and the dependence on the choice of collinear gluon distribution functions for the KMR UGDF (right). The results of calculation are compared with the LHCb Collaboration data.

distributions. We show now also results for charm meson pseudorapidity distributions. In Figs. 20 and 21, we show pseudorapidity distributions for the charged $D^{\pm}$ meson. These distributions are rather flat. The results are also compared to recent (preliminary) ATLAS data. Only the upper limits of large error bars of the theoretical results obtained with the KMR distributions are consistent with the ATLAS data. The results with other UGDFs clearly underpredict the experimental data.

As for pseudoscalar mesons above, in Fig. 22, we show transverse momentum distributions for charged vector mesons. The situation is pretty much the same as for pseudoscalar charged mesons discussed previously in Figs. 18 and 19.

In Fig. 21, we compare results obtained within the k_t-factorization approach (gray band) with results obtained within other approaches. The central value of the k_t-factorization approach with the KMR UGDF is consistent with the FONLL and NLO PM predictions.

In Fig. 23, we show also results of the KKKS08 fragmentation function which includes evolution. The conclusions are the same as for ALICE conditions.

C. LHCb

Finally, let us focus on the measurements in the forward rapidity region $2 < y < 4.5$. Recently, the LHCb Collaboration presented first results for the production of D^0, D^+, D^{*+}, and D_s^+ mesons [22]. In this region of phase space, one tests asymmetric gluon longitudinal momentum fractions: $x_1 \sim 10^{-5}$ and $x_2 > 10^{-2}$ (see Fig. 2). This is certainly a more difficult region for reliable calculation and interpretation of experimental data. First of all, gluon

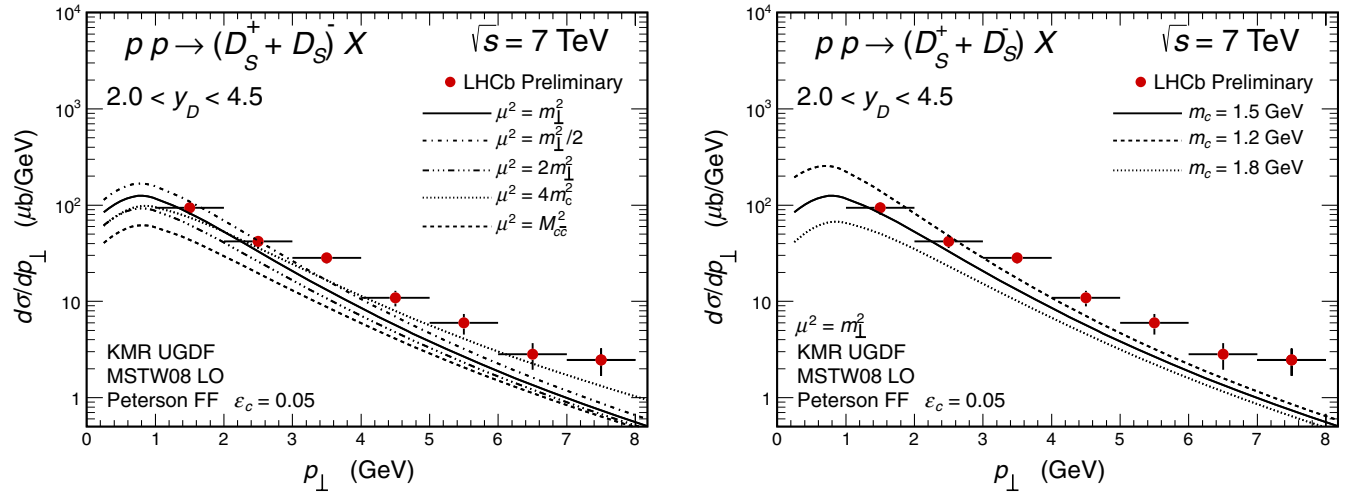

FIG. 25 (color online). Uncertainties of the theoretical predictions due to the choice of scales for the KMR UGDF (left) and due to charm quark mass (right).

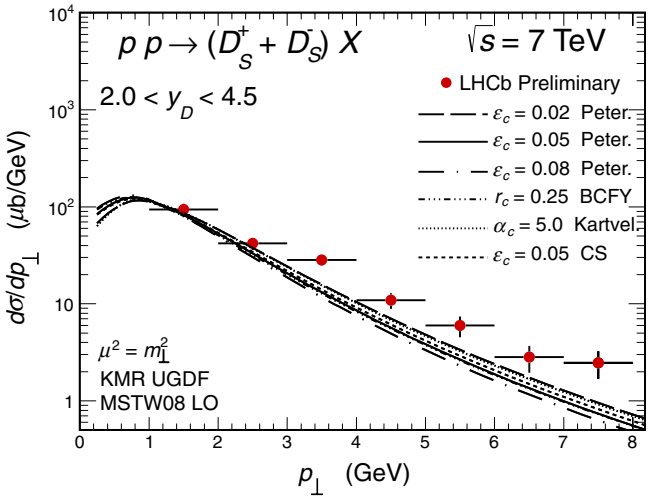

FIG. 26 (color online). Uncertainties in the fragmentation of $c \to D_s^+$. We show results obtained with different fragmentation functions from the literature.

distributions were never tested at such small x_1 values. Second, many UGDFs from the literature may be not good enough for $x_2 > 10^{-2}$. Therefore, some care in interpreting the results is required.

The LHCb, similar as ALICE, has measured also distributions of rather rarely produced D_s^+ mesons. We start from transverse momentum distributions for $D_s^\pm$ mesons. In Fig. 24, we present distributions for different UGDFs from the literature and uncertainties for the KMR UGDF related to the choice of standard PDFs. In Fig. 25, we show uncertainties related to the choice of factorization or renormalization scale and due to the choice of quark masses and in Fig. 26 uncertainties related to fragmentation functions. All these uncertainties are very similar as for the ALICE and ATLAS kinematics.

In Fig. 27, we compare our predictions, together with predictions of other popular approaches. The main conclusions are the same again as for the ALICE and ATLAS. In Fig. 28, we show also results of the KKKS08 fragmentation function which includes evolution. The conclusions are the same as for ALICE and ATLAS conditions.

The LHCb Collaboration was able to measure transverse momentum distributions of mesons in many narrow bins of (pseudo)rapidity. Below (Figs. 29–31), we show such distributions for D^0, D^+, and D^{*+}, respectively. In general, different bins are sensitive to different regions of longitudinal momentum fractions carried by gluons. However, we do not observe any interesting trend in the quality of the description of the LHCb data. Our results with the KMR UGDF within uncertainties are consistent with the experimental data and with the FONLL and NLO PM predictions. Corresponding distributions for PYTHIA are taken from Ref. [22] and have a slightly different p_t slope than the other ones.

VI. PRODUCTION OF $D\bar{D}$ PAIRS

Most of the calculations in the literature concentrate on single meson distributions. We focus now on correlation observables for D and $\bar{D}$ mesons. In order to calculate correlation observables for two mesons, we follow here, similar as in the single meson case, the fragmentation function technique for the hadronization process:

$$\frac{d\sigma(pp \to D\bar{D}X)}{dy_1 dy_2 d^2p_{1t}^D d^2p_{2t}^{\bar{D}}} \approx \int \frac{D_{c\to D}(z_1)}{z_1} \cdot \frac{D_{\bar{c}\to\bar{D}}(z_2)}{z_2} \cdot \frac{d\sigma(pp \to c\bar{c}X)}{dy_1 dy_2 d^2p_{1t}^c d^2p_{2t}^{\bar{c}}} dz_1 dz_2, \tag{6.1}$$

where $p_{1t}^c = \frac{p_{1,t}^D}{z_1}$, $p_{2,t}^{\bar{c}} = \frac{p_{2t}^{\bar{D}}}{z_2}$, and meson longitudinal fractions $z_1, z_2 \in (0, 1)$. The multidimensional distribution for

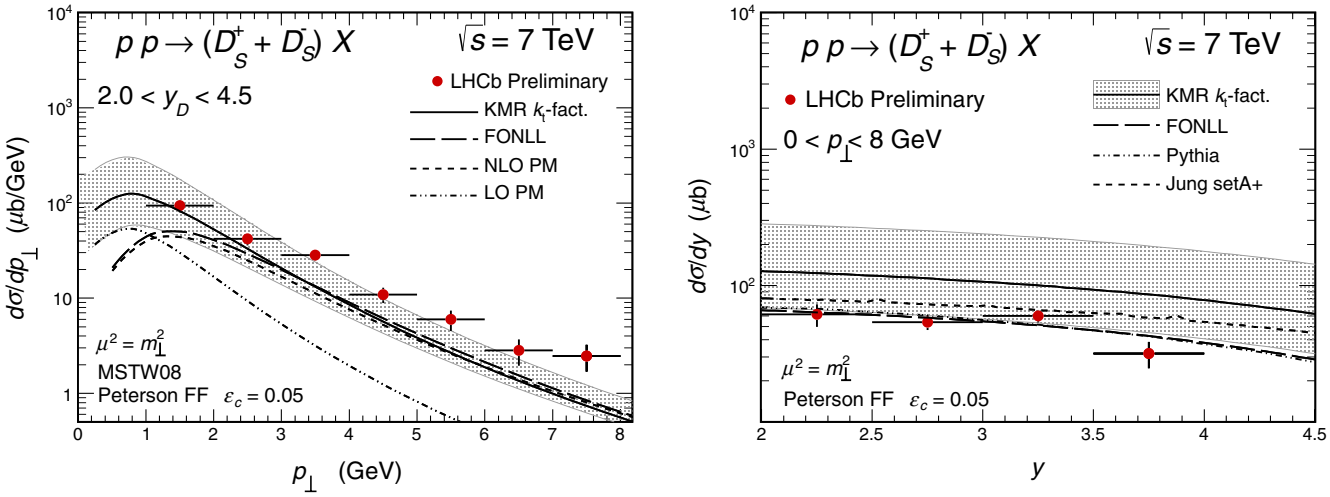

FIG. 27 (color online). Results with overall uncertainties for transverse momentum (left) and rapidity distributions (right) of $D_s^\pm$ for the k_t-factorization approach with the KMR UGDF. For comparison we show predictions of other popular approaches.

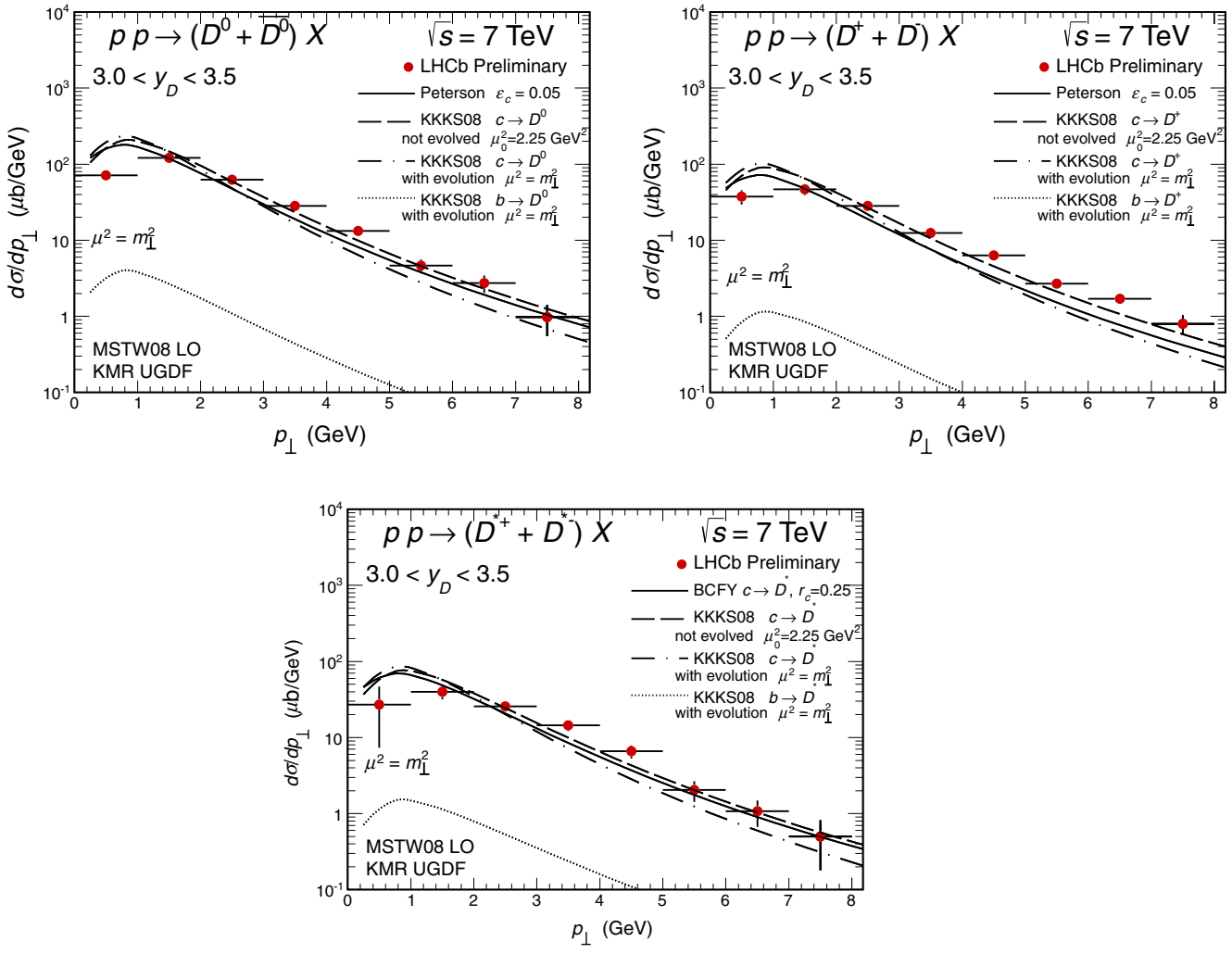

FIG. 28 (color online). Effect of the evolution of the fragmentation functions for D^0, D^+, and D^* for the LHCb kinematics. We compare results obtained with the KKKS08 fragmentation function with the other commonly used functions. The $b \to D$ contribution is shown in addition. The details are specified in the figures.

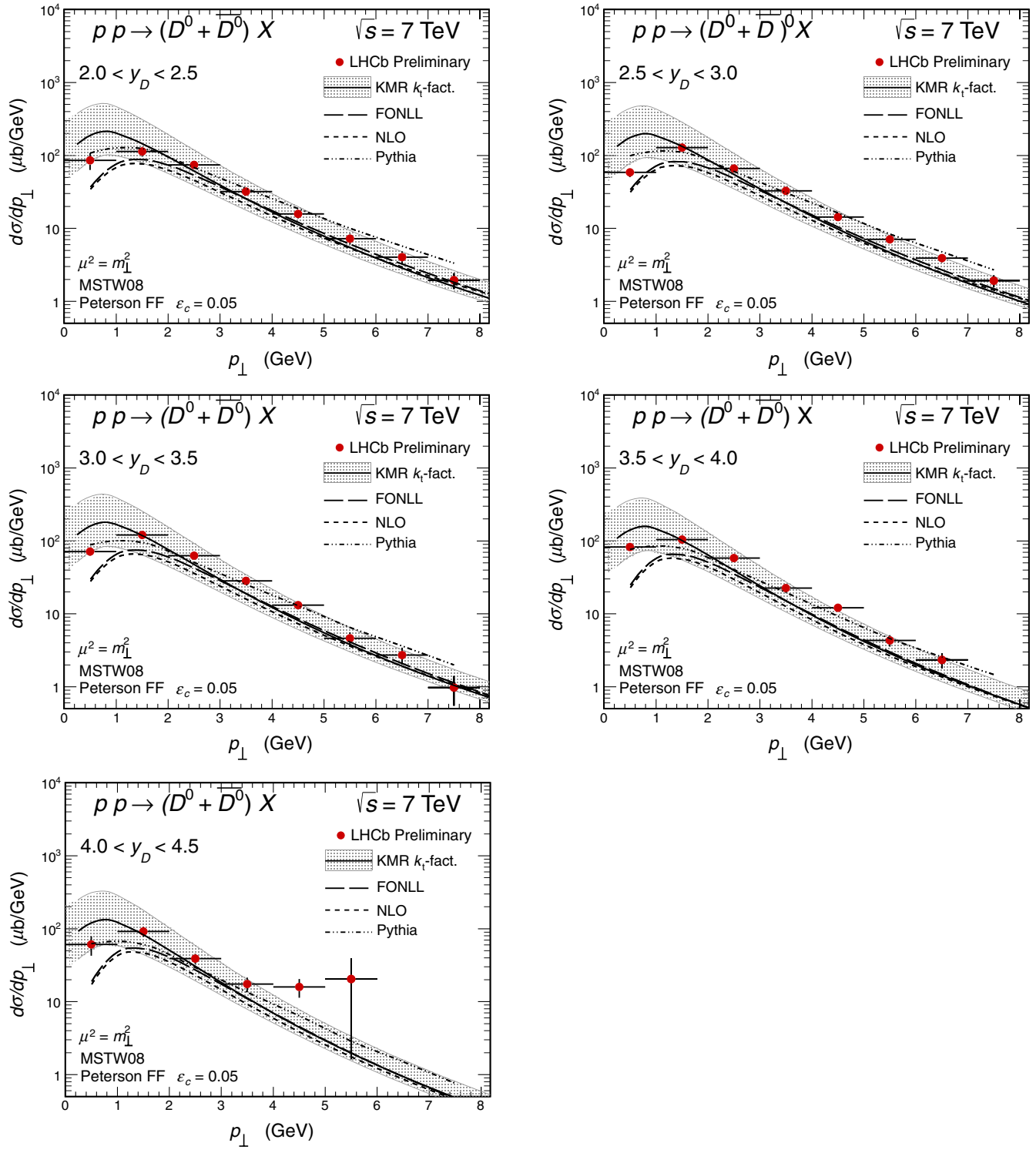

FIG. 29 (color online). Transverse momentum distribution of neutral D^0 mesons for different ranges of rapidities specified in the figures. We compare results of the k_t-factorization approach with the KMR UGDF and those obtained within other approaches known from the literature.

the c quark and $\bar{c}$ antiquark is convoluted with respective fragmentation functions simultaneously. As a result of the hadronization, one obtains corresponding two-meson multidimensional distribution. In the last step, experimental kinematical cuts on the distributions can be imposed. Then the resulting distributions can be compared with experimental ones. For numerical calculations, here we again apply the Peterson model of fragmentation function [42].

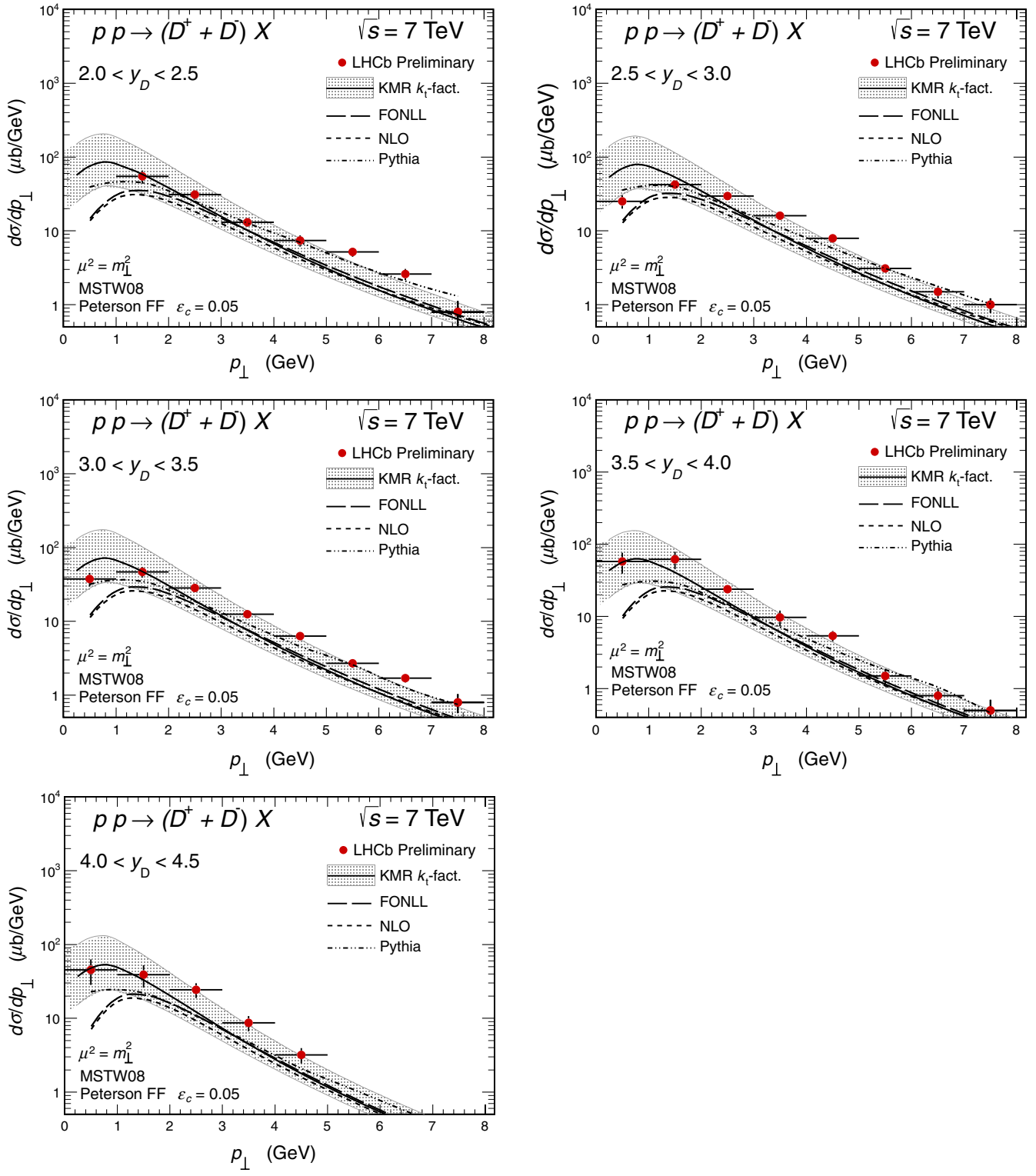

FIG. 30 (color online). Transverse momentum distribution of charged D^+ mesons for different ranges of rapidities specified in the figures. We compare results of the k_t-factorization approach with the KMR UGDF and those obtained within other approaches known from the literature.

The experimental cross sections for the production of two mesons are also (or even a bit more) sensitive to the details of hadronization as it was in the cases of the inclusive single D meson production discussed in the previous section. For example, in Fig. 32, we compare the transverse momentum distribution of the D^0 meson provided that $\bar{D}^0$ is also measured for two different values of the ε_c parameter of the Peterson fragmentation function.

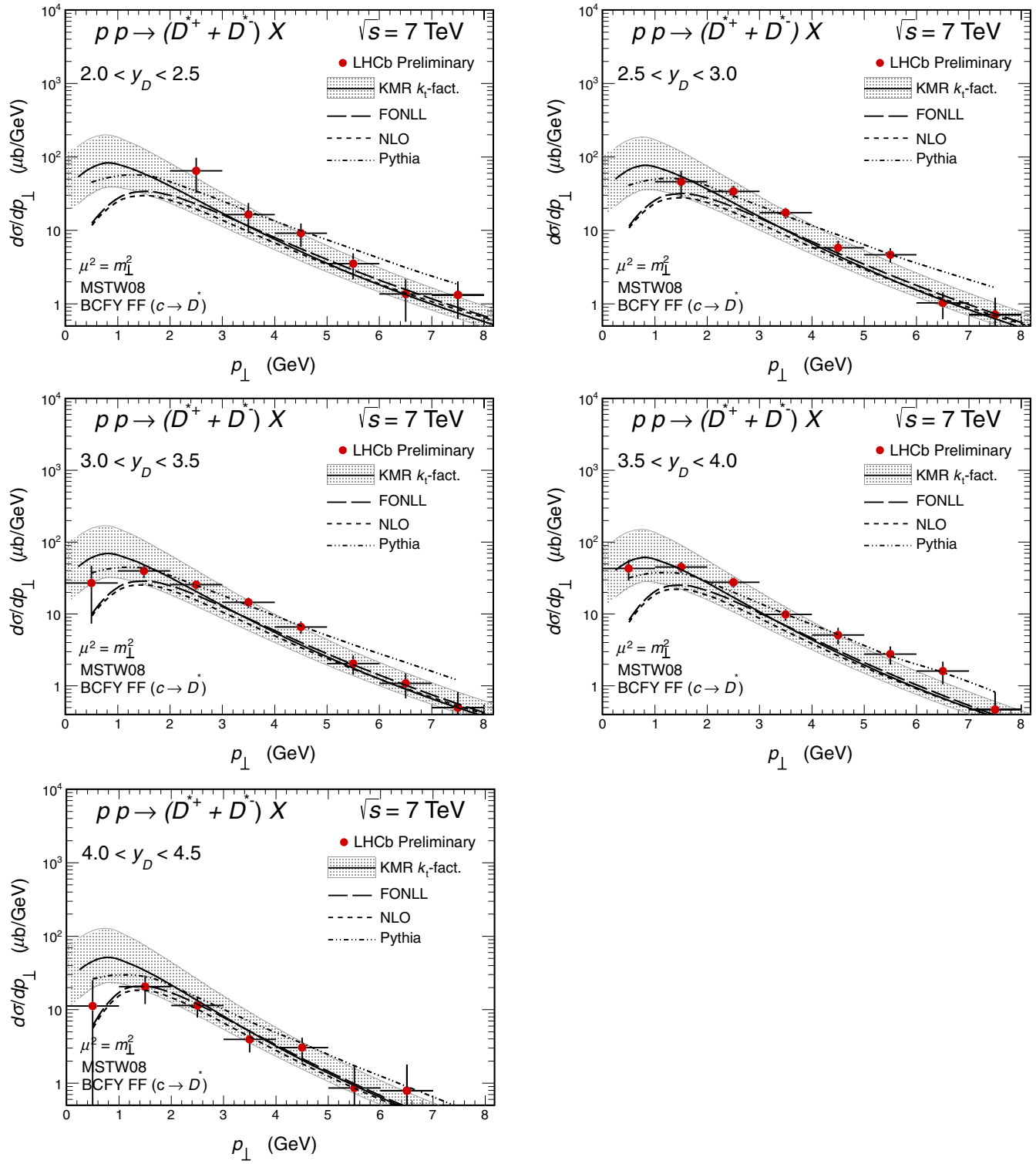

FIG. 31 (color online). Transverse momentum distribution of D^{*+} mesons for different ranges of rapidities specified in the figures. We compare results of the k_t-factorization approach with the KMR UGDF and those obtained within other approaches known from the literature.

The larger the meson transverse momentum, the larger the sensitivity to the value of ε_c. For illustration, we show the range of transverse momenta relevant for the recent experiments of the LHCb Collaboration [23]. The effect of the modification of the ε_c from 0.05 to 0.02 is quite sizable. In the LHCb acceptance, it does not really affect the shape of the calculated p_t distribution but has an important effect for the predictions of integrated cross sections. In Table II,

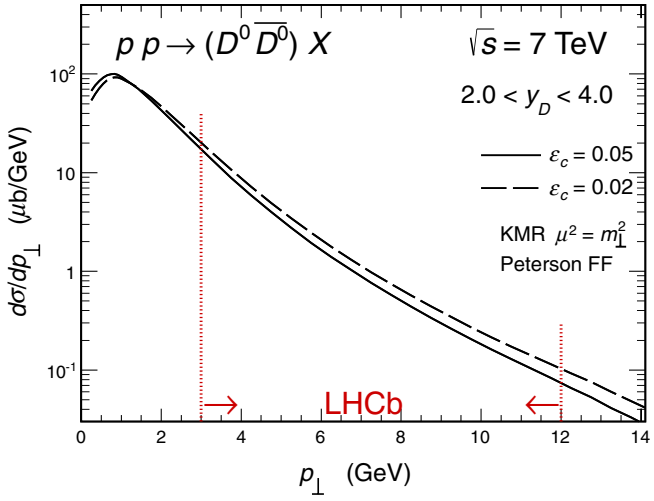

FIG. 32 (color online). Transverse momentum of the D^0 meson within the LHCb acceptance provided that $\bar{D}^0$ was registered, too. Here the KMR UGDF was used. We show results for different values of the Peterson fragmentation function parameter ε_c.

we compare cross sections measured by the LHCb Collaboration for different $D\bar{D}$ modes with our theoretical results. Calculated values for three different UGDFs are consistent with the measured ones, taking into account rather large experimental and theoretical uncertainties. In particular, this is true only when $\varepsilon_c = 0.02$ is taken in the calculation of the fragmentation process. Results obtained with the KMR UGDF are the closest to the experimental numbers.

In Fig. 33, we present transverse momentum distributions of the D^0 meson for the case when $D^0\bar{D}^0$ pairs are counted. We compare theoretical distributions for different UGDFs (left panel) as well as discuss effect of the scale dependence (right panel) on the shape of the p_t distribution. The experimental data points are normalized by a factor of $1/\sigma$. The shape of the transverse momentum distribution is rather well reproduced by all UGDFs used. The normalization, as discussed already in Table II, is less consistent.

The LHCb Collaboration presented also distribution in the $D^0\bar{D}^0$ invariant mass $M_{D^0\bar{D}^0}$. In Fig. 34, we show the corresponding theoretical result for different UGDFs. Both the KMR and KMS UGDFs provide the right shape of the distribution. The dip at small invariant masses is due to specific LHCb cuts on kinematical variables. On the other hand, the shape of the distribution almost does not depend on the choice of the scales for the KMR UGDF (see the right panel).

The LHCb detector has almost full coverage in azimuthal angle. In Fig. 35, we discuss distribution in azimuthal angle between the D^0 and $\bar{D}^0$ mesons $\varphi_{D^0\bar{D}^0}$. Again, the KMR and KMS distributions give a quite reasonable description of the shape of the measured distribution. Both of them give the enhancement of the cross section at $\phi_{D\bar{D}} \sim 0$. This is due to the fact that these approaches include an effectively gluon splitting contribution, not included in the case of the Jung UGDFs. This was also discussed in Ref. [8], where additional calculations of the $g^*g^* \to gg \to gc\bar{c}$ subprocess in the case of the Jung UGDFs were performed to describe azimuthal angle correlation between D and $\bar{D}$ mesons measured at the Tevatron. Some dependence of the shape on the choice of the factorization or renormalization scale in the case of the KMR UGDF can be also observed (see the right panel). However, still even with the KMR UGDF, one can observe some small missing strength at small angles. It may suggest that within the KMR model the gluon splitting contribution is not fully included.

In order to better understand the result for the azimuthal correlations, in Fig. 36, we show two-dimensional distributions in invariant mass $M_{D^0\bar{D}^0}$ and azimuthal angle between mesons $\varphi_{D^0\bar{D}^0}$. The maximum obtained for the KMR UGDF for the small relative azimuthal angle between D and $\bar{D}$ mesons corresponds to small invariant masses of the $D^0\bar{D}^0$ system. This strongly supports the interpretation of the effect as the gluon splitting into a $c\bar{c}$ pair. However, one can also see that these interesting shapes of the correlation observable are the consequence of the specific LHCb kinematical cuts.

VII. SUMMARY

First, we have discussed the general situation with the $c\bar{c}$ production at LHC energies. We have argued that the $c\bar{c}$ production is related with small-x physics. Therefore, it has a good potential to test different models of unintegrated gluon distributions.

TABLE II. Integrated cross sections for the two meson modes specified in the table below within the LHCb detector.

		$\sigma_{\rm tot}^{\rm THEORY}$ [nb]					
		KMR$^{+}_{-}(\mu)^{+}_{-}(m_c)$		Jung setA+		KMS	
Mode	$\sigma_{\rm tot}^{\rm EXP}$[nb]	$\varepsilon_c = 0.05$	$\varepsilon_c = 0.02$	$\varepsilon_c = 0.05$	$\varepsilon_c = 0.02$	$\varepsilon_c = 0.05$	$\varepsilon_c = 0.02$
$D^0\bar{D}^0$	$6230 \pm 120 \pm 630$	$5193\ ^{+1346}_{-879}\ ^{+654}_{-576}$	6971	4532	5814	2895	3894
D^0D^-	$3990 \pm 90 \pm 500$	$4155\ ^{+1076}_{-704}\ ^{+523}_{-461}$	5577	3626	4652	2316	3115
$D^0D_S^-$	$1680 \pm 110 \pm 240$	$1471\ ^{+381}_{-249}\ ^{+185}_{-163}$	1974	1284	1647	820	1103
D^+D^-	$780 \pm 40 \pm 130$	$831\ ^{+215}_{-141}\ ^{+105}_{-92}$	1115	725	930	463	623
$D^+D_S^-$	$550 \pm 60 \pm 90$	$588\ ^{+152}_{-99}\ ^{+74}_{-65}$	790	513	659	328	441
$D_S^+D_S^-$	$\cdots$	$104\ ^{+27}_{-17}\ ^{+13}_{-11}$	139	91	117	59	78

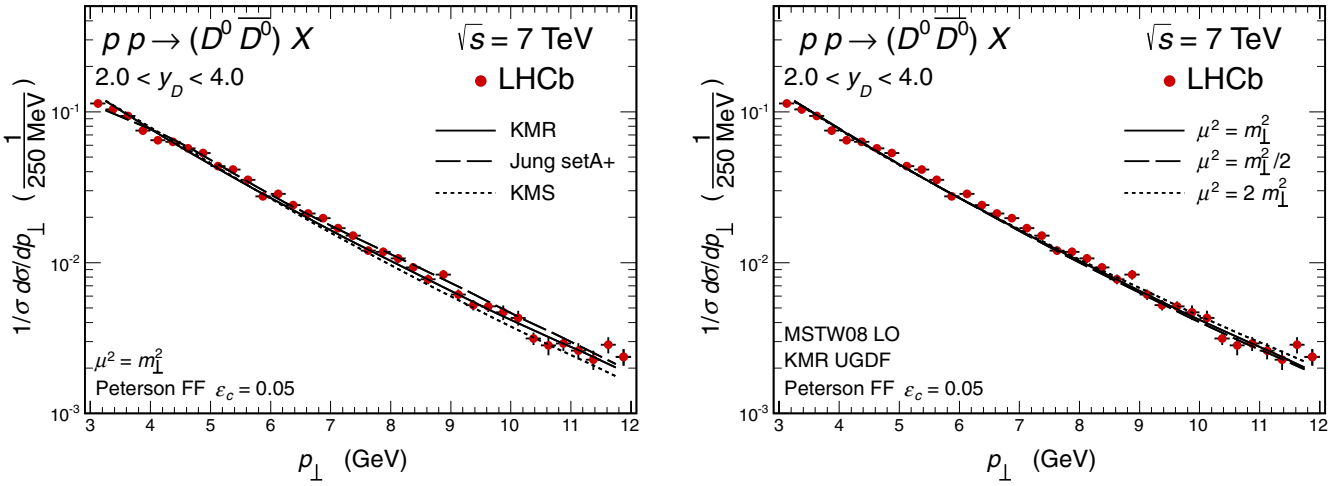

FIG. 33 (color online). Uncertainties for the conditional transverse momentum distribution due to the choice of UGDF model (left) and due to the choice of scales for the KMR UGDF (right). The experimental data of the LHCb Collaboration are from Ref. [23].

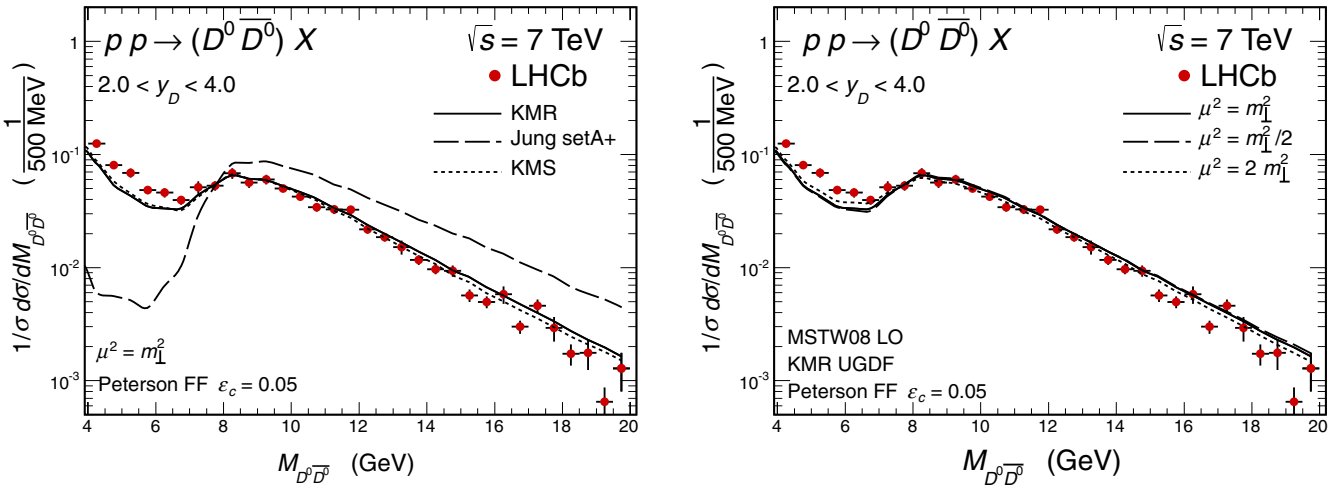

FIG. 34 (color online). Invariant mass distribution of the $D^0\bar{D}^0$ system for different UGDFs (left) and uncertainties due to the choice of the scale for the KMR UGDF (right). The experimental data of the LHCb Collaboration are taken from Ref. [23].

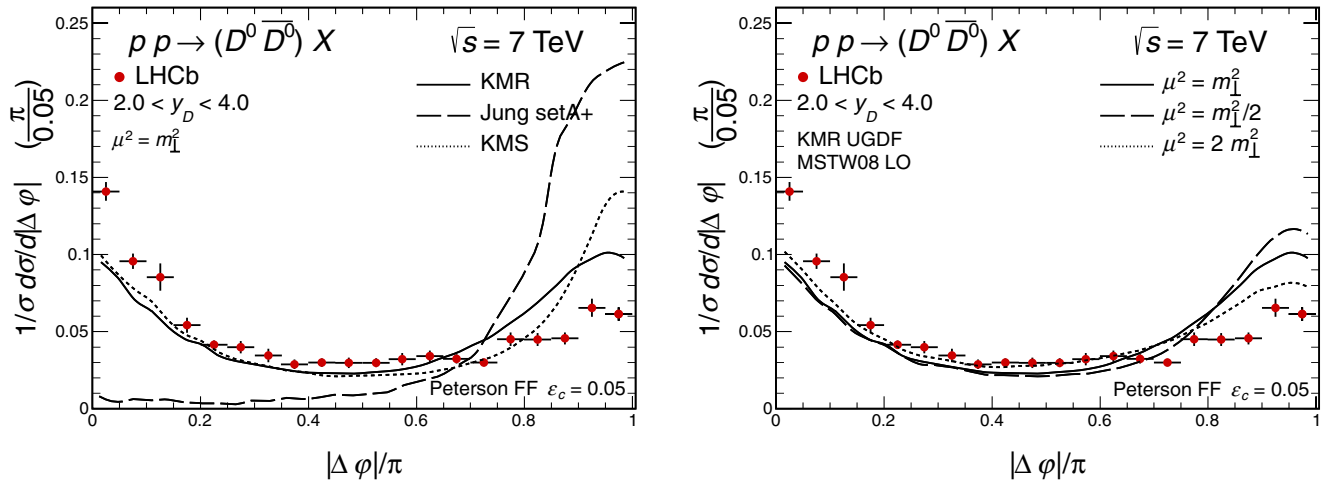

FIG. 35 (color online). Distribution in relative azimuthal angle between D^0 and $\bar{D}^0$ for different UGDFs (left) and uncertainties due to the choice of the scale for the KMR UGDF (right).

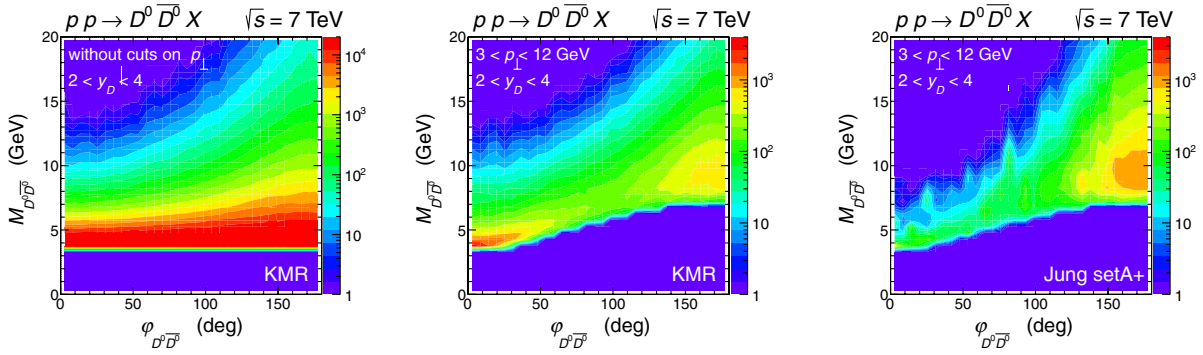

FIG. 36 (color online). Two-dimensional distribution in $D\bar{D}$ invariant mass and relative azimuthal angle between D and $\bar{D}$ for the KMR and Jung setA+ UGDFs.

In the present paper, we have focused on production of D mesons at the LHC within the k_t-factorization formalism with unintegrated gluon distributions. Only the Kimber-Martin-Ryskin unintegrated gluon distribution gives transverse momentum distributions of charmed mesons similar to the recently measured ones by the ATLAS, ALICE, and LHCb Collaborations. Our inclusive theoretical distributions with the KMR UGDFs are very similar to those obtained within FONLL or NLO approaches. All other unintegrated gluon distributions strongly underpredict the experimental results. This may suggest that some mechanism of charm production is still missing. In a parallel paper [55], we discuss double parton scattering effects as a potential missing mechanism.

The issue of testing of UGDFs is somewhat related with the choice of fragmentation functions. In the present work, we have used many fragmentation functions from the literature. Most of them do not include QCD evolution. The results with the Kneesch-Kniehl-Kramer-Schienbein fragmentation function, which include DGLAP evolution, give somewhat smaller cross sections at large meson transverse momenta. This may point to some missing higher-order mechanisms of charm production or inconsistency of using these fragmentation functions within our k_t-factorization approach.

Recently, the LHCb Collaboration has presented first results for D and $\bar{D}$ meson two-particle distributions. We have presented first theoretical results for such observables. Our model calculation with the KMR UGDF relatively well describes both $D\bar{D}$ meson invariant mass distributions as well as $D\bar{D}$ correlations in relative azimuthal angle between the meson and antimeson. This shows that the k_t-factorization approach is very efficient in describing the two-particle distributions. In contrast, the NLO QCD approach can be used only in a limited region of the phase space, but no real results have been presented so far in the literature.

ACKNOWLEDGMENTS

We are indebted to Vanya Belyaev and Marek Szczekowski for the discussion concerning recent results at the LHC. This study was partially supported by the Polish Grants No. DEC-2011/01/B/ST2/04535 and No. N202 237040.

[1] P. Nason, S. Dawson, and R. K. Ellis, Nucl. Phys. **B303**, 607 (1988); **B327**, 49 (1989); W. Beenakker, H. Kuijf, W. van Neerven, and J. Smith, Phys. Rev. D **40**, 54 (1989); Nucl. Phys. **B351**, 507 (1991).

[2] M. Cacciari, M. Greco, and P. Nason, J. High Energy Phys. 05 (1998) 007; M. Cacciari, S. Frixione, and P. Nason, J. High Energy Phys. 03 (2001) 006.

[3] B. A. Kniehl, G. Kramer, I. Schienbein, and H. Spiesberger, Phys. Rev. D **71**, 014018 (2005); Phys. Rev. Lett. **96**, 012001 (2006); Phys. Rev. D **79**, 094009 (2009).

[4] Ph. Hägler, R. Kirschner, A. Schäfer, I. Szymanowski, and O. V Teryaev, Phys. Rev. D **62**, 071502 (2000).

[5] S. P. Baranov and M. Smizanska, Phys. Rev. D **62**, 014012 (2000).

[6] S. P. Baranov, A. V. Lipatov, and N. P. Zotov, Yad. Fiz. **67**, 856 (2004) [Phys. At. Nucl. **67**, 837 (2004)].

[7] Yu. M. Shabelski and A. G. Shuvaev, Phys. At. Nucl. **69**, 314 (2006).

[8] H. Jung, M. Kraemer, A. V. Lipatov, and N. P. Zotov, J. High Energy Phys. 01 (2011) 085.

[9] H. Jung, M. Kraemer, A. V. Lipatov, and N. P. Zotov, Phys. Rev. D **85**, 034035 (2012).

[10] B. A. Kniehl, V. A. Saleev, and A. V. Shipilova, Phys. Rev. D **79**, 034007 (2009); **81**, 094010 (2010).

[11] V. A. Saleev and A. V. Shipilova, Phys. Rev. D **86**, 034032 (2012).
[12] M. A. Kimber, A. D. Martin, and M. G. Ryskin, Phys. Rev. D **63**, 114027 (2001); G. Watt, A. D. Martin, and M. G. Ryskin, Eur. Phys. J. C **31**, 73 (2003).
[13] J. Kwieciński, A. D. Martin, and A. M. Staśto, Phys. Rev. D **56**, 3991 (1997).
[14] K. Kutak and A. M. Stasto, Eur. Phys. J. C **41**, 343 (2005).
[15] H. Jung and G. P. Salam, Eur. Phys. J. C **19**, 351 (2001); H. Jung, arXiv:hep-ph/0411287.
[16] K. Golec-Biernat and M. Wüsthoff, Phys. Rev. D **60**, 114023 (1999).
[17] M. Łuszczak, R. Maciuła, and A. Szczurek, Phys. Rev. D **79**, 034009 (2009).
[18] R. Maciuła, A. Szczurek, and G. Ślipek, Phys. Rev. D **83**, 054014 (2011).
[19] ATLAS Collaboration, Report No. ATLAS-CONF-2011-017.
[20] ALICE Collaboration, J. High Energy Phys. 01 (2012) 128.
[21] ALICE Collaboration, Report No. CERN-PH-EP-2012-227; ALICE CollaborationPhys. Lett. B **718**, 279 (2012).
[22] LHCb Collaboration, Report No. LHCb-CONF-2010-013.
[23] LHCb Collaboration, J. High Energy Phys. 06 (2012) 141.
[24] STAR Collaboration, Phys. Rev. Lett. **105**, 202301 (2010); A. Mischke, Phys. Lett. B **671**, 361 (2009).
[25] CDF Collaboration, Report No. FERMILAB-CONF-07-634-E.
[26] S. Catani, M. Ciafaloni, and F. Hautmann, Nucl. Phys. **B366**, 135 (1991).
[27] J. C. Collins and R. K. Ellis, Nucl. Phys. **B360**, 3 (1991).
[28] R. D. Ball and R. K. Ellis, J. High Energy Phys. 05 (2001) 053.
[29] M. Łuszczak and A. Szczurek, Phys. Lett. B **594**, 291 (2004).
[30] A. V. Lipatov and N. P. Zotov, Eur. Phys. J. C **47**, 643 (2006).
[31] A. V. Lipatov and N. P. Zotov, Phys. Rev. D **75**, 014028 (2007).
[32] A. Leonidov and D. Ostrovsky, Phys. Rev. D **62**, 094009 (2000).
[33] A. Szczurek, A. Rybarska, and G. Ślipek, Phys. Rev. D **76**, 034001 (2007).
[34] A. van Hameren, P. Kotko, and K. Kutak, J. High Energy Phys. 12 (2012) 029.
[35] K. Kutak and S. Sapeta, Phys. Rev. D **86**, 094043 (2012).
[36] M. Deak, F. Hautmann, H. Jung, and K. Kutak, Eur. Phys. J. C **72**, 1982 (2012); arXiv:1012.6037.
[37] G. Watt, A. D. Martin, and M. G. Ryskin, Phys. Rev. D **70**, 014012 (2004); **70**, 079902(E) (2004).
[38] E. N. Antonov, L. N. Lipatov, and E. A. Kuraev, Nucl. Phys. **B721**, 111 (2005).
[39] M. Cacciari, S. Frixione, N. Houdeau, M. L. Mangano, P. Nason, and G. Ridolfi, J. High Energy Phys. 10 (2012) 137.
[40] B. A. Kniehl, G. Kramer, I. Schienbein, and H. Spiesberger, Eur. Phys. J. C **72**, 2082 (2012).
[41] M. Łuszczak and A. Szczurek, Phys. Rev. D **73**, 054028 (2006).
[42] C. Peterson, D. Schlatter, I. Schmitt, and P. M. Zerwas, Phys. Rev. D **27**, 105 (1983).
[43] M. Cacciari, P. Nason, and R. Vogt, Phys. Rev. Lett. **95**, 122001 (2005).
[44] E. Braaten, K. Cheung, S. Fleming, and T. C. YuanPhys. Rev. D **51**, 4819 (1995).
[45] V. G. Kartvelishvili, A. K. Likhoded, and V. A. Petrov, Phys. Lett. **78B**, 615 (1978).
[46] P. D. B. Collins and T. P. Spiller, J. Phys. G **11**, 1289 (1985).
[47] E. Lohrmann, arXiv:1112.3757.
[48] J. Binnewies, B. A. Kniehl, and G. Kramer, Z. Phys. C **65**, 471 (1995); **76**, 677 (1997); Phys. Rev. D **53**, 6110 (1996); B. A. Kniehl, G. Kramer, and B. Potter, Nucl. Phys. **B582**, 514 (2000); B. A. Kniehl and G. Kramer, Phys. Rev. D **71**, 094013 (2005); **74**, 037502 (2006); S. Albino, B. A. Kniehl, and G. Kramer, Nucl. Phys. **B725**, 181 (2005).
[49] T. Kneesch, B. A. Kniehl, G. Kramer, and I. Schienbein, Nucl. Phys. **B799**, 34 (2008).
[50] A. D. Martin, W. J. Stirling, R. S. Thorne, and G. Watt, Eur. Phys. J. C **63**, 189 (2009); **64**, 653 (2009).
[51] J. Pumplin, D. R. Stump, J. Huston, H.-L. Lai, P. Nadolsky, and W.-K. Tung, J. High Energy Phys. 07 (2002) 012; H. L. Lai, Phys. Rev. D **82**, 054021 (2010).
[52] M. Glück, D. Jimenez-Delgado, and E. Reya, Eur. Phys. J. C **53**, 355 (2008).
[53] M. Glück, E. Reya, and A. Vogt, Eur. Phys. J. C **5**, 461 (1998).
[54] M. Łuszczak, R. Maciuła, and A. Szczurek, Phys. Rev. D **84**, 114018 (2011).
[55] R. Maciuła and A. Szczurek, Phys. Rev. D **87**, 074039 (2013).